Nucleolin is essential for rabbit hemorrhagic disease virus replication by providing a physical link in replication complex formation

Jie Zhu[1], Qiuhong Miao[1, 2], Hongyuan Guo[1], Ruibin Qi[1], Aoxing Tang[1], Dandan Dong[1], Jingyu Tang[1], Guangzhi Tong[1*], Guangqing Liu[1*]

[1] Shanghai Veterinary Research Institute, Chinese Academy of Agricultural Sciences, Shanghai, 200241, China;

[2] Laboratory of Virology, Wageningen University and Research, Wageningen, 6708 PB, The Netherlands;

[*]Corresponding author

E-mail: liugq@shvri.ac.cn (GL); gztong@shvri.ac.cn (GT)

Abstract

Rabbit hemorrhagic disease virus (RHDV) is an important member of the *Caliciviridae* family and cannot be propagated *in vitro*, which has greatly impeded progress of investigating its replication mechanism. Construction of an RHDV replicon system has recently provided a platform for exploring RHDV replication in host cells. Here, aided by this replicon system and using two-step affinity purification, we purified the RHDV replicase and identified its associated host factors. We identified rabbit nucleolin (NCL) as a physical link required for the formation of RHDV replication complexes (RCs), by mediating the interaction between other host proteins and the viral RNA replicase, RNA-dependent RNA polymerase (RdRp). We found that RHDV RdRp uses an amino acid (aa) region spanning residues 448–478 to directly interact with NCL's RNA-recognition motif 2. We also found that the viral p16 protein uses a highly conserved region (^{35}Cys–Ile–Arg–Ala^{38} or CIRA motif) to specifically bind the N-terminal region of NCL (aa 1–110) and that RHDV p23 uses a specific domain (aa 90–145) to bind NCL's RNA-recognition motif 1. Disrupting these protein–protein interactions severely weakened viral replication. Furthermore, NCL overexpression or knockdown significantly increased or severely impaired, respectively, RHDV replication. Collectively, these results indicate that the host protein NCL is essential for RHDV replication and plays a key role in the formation of RHDV RCs. The mechanisms by which NCL promotes viral replicase assembly reported here shed light on viral RC biogenesis and may inform antiviral therapies.

Author summary

Rabbit hemorrhagic disease virus (RHDV) is the causative agent of highly contagious and lethal hemorrhagic disease in the European rabbit, but the host factors involved in RHDV replication remain poorly understood. In the present study, we isolated RHDV replication complex (RC) for the first time and identified its main components. We found that nucleolin (NCL) plays a key role in the formation of the RHDV RC. NCL not only interacts with viral replicase (RdRp), it also specifically binds to other important host factors. In addition, we proved that NCL is necessary for RHDV replication because the level of RHDV replication is significantly affected by knocking down the NCL gene in cells. Together, our data suggest that RHDV completes its replication by hijacking NCL to recruit other viral proteins and host factors, thereby assembling the RC of RHDV.

Introduction

Rabbit hemorrhagic disease virus (RHDV) is the causative agent of rabbit hemorrhagic disease (RHD), which primarily infects the wild and domestic European rabbit (*Orcytolagus cuniculus*) [1] and is characterized by liver degeneration, diffuse hemorrhaging and high mortality [2,3]. However, the molecular mechanisms responsible for RHDV replication remain poorly understood, mainly due to the lack of a robust cell culture system for propagation of the virus.

RHDV is a nonenveloped positive-sense single-stranded RNA virus, which belongs to the family *Caliciviridae*, genus *Lagovirus*. RHDV virions contain the genomic RNA (gRNA) and an additional 2.2 kb of subgenomic RNA (sgRNA), which is collinear with the 3′ end of the gRNA [1]. The gRNA of RHDV consists of a positive-sense single-stranded molecule of 7,437 nucleotides with a virus-encoded protein, VPg, which is covalently attached to its 5′ end [4,5]. The gRNA also contains two slightly overlapping open reading frames (ORFs) of 7

kb (ORF1) and 351 nucleotides (ORF2). ORF1 is translated into a large polyprotein that is cleaved into the major structural protein VP60, the capsid protein, and seven nonstructural proteins: p16, p23, helicase, p29, VPg, protease, and RNA-dependent RNA polymerase (RdRp). ORF2 encodes the minor structural protein VP10 [6-8]. The sgRNA, which only encodes VP60 and VP10, usually contributes to the production of high levels of products required during intermediate and late stages of infection [9]. Flanking the coding regions of RHDV is a 5′ terminal noncoding region of nine nucleotides and a 3′ terminal noncoding region of 59 nucleotides [8].

The function of some of the nonstructural proteins encoded by the genome of caliciviruses has been identified and/or predicted by relying on previous knowledge gathered from members of the closely related *Picornaviridae* family. For RHDV, two nonstructural proteins might be involved in the replication of viral RNA, a helicase and an RdRp, and a protease is involved in the autoproteolytic processing of the large viral polyprotein encoded by ORF1 [7,10,11]. The genome-binding protein VPg is covalently linked to both genomic and subgenomic RHDV RNAs at the 5’ end. Our previous study suggested that the VPg protein serves as a novel cap substitute during the initiation of RHDV translation [5]; however, the precise function of the RHDV nonstructural proteins (p16, p23, and p29) remains unclear.

Following attachment of RHDV to the cell surface, internalization and desencapsidation occur, leading to release of the viral genome into the cytoplasm of the host cell. The virus life cycle then proceeds to translation of the polyprotein precursor encoded by the viral genome through interaction with the host cellular machinery. The gRNA and the sgRNA covalently-linked VPg use the cellular translation machinery, positioning the ribosome at the start codon AUG without ribosome scanning and initiating translation. Posttranslational proteolytic processing by the viral gRNA encoded protease cleaves the polyprotein precursor into the

mature nonstructural proteins and, in RHDV, into the capsid protein VP60. The nonstructural proteins, helicase and RdRp, then form a replication complex (RC), synthesizing complementary negative-sense RNA from the gRNA, which is used as a template for the synthesis of gRNA and sgRNA.

The positive-strand RNA viruses share a conserved replication mechanism in which viral proteins induce host cell membrane modification to assemble membrane-associated viral RC [12]. Viruses hijack host factors to facilitate this energy-consuming process [13]. However, understanding the detailed molecular mechanism of how viral proteins hijack host factors for RC assembly has been hampered by the lack of a suitable *in vitro* culture system for RHDV. Identification of replicase-associated host factors and dissection of their roles in RC assembly will shed light on the molecular mechanism of RHDV replication. In 2013, we developed an RHDV replicon system, which has the ability to automatically replicate in RK-13 cells [14]. Construction of this RHDV replicon system has provided a platform for exploring RHDV replication in host cells. In 2017, we successfully constructed mutant RHDV (mRHDV) in RK-13 cells *in vitro*, which has a specific receptor-recognition motif (Arg-Gly-Asp) on the surface of the capsid protein that is characterized by two aa substitutions. mRHDV is recognized by the intrinsic membrane receptor (integrin α3β1) of RK-13 cells, by which mRHDV gains entry, replicates, and imparts apparent cytopathic effects [15].

In this study, an RHDV RC was isolated for the first time and its main components were identified. We found that nucleolin (NCL) plays a key role in the formation of viral RCs. Our data showed that NCL is a link between viral replicase and host proteins. In addition, we demonstrated that NCL is necessary for RHDV replication because the replication level of RHDV is significantly affected by knocking down the *NCL* gene in cells.

Results

Tagging of RHDV replicase (RdRp) in the context of a viral replicon

To discover the host factors that are involved in RHDV replication, we attempted to purify the viral RCs formed during viral replication and identify the associated host factors. Previously, the researchers successfully identified hepatitis C virus (HCV) replicase-associated RC components by inserting His and HA tags into the HCV replicon replicase NS5A and NS5B (RdRp) for affinity purification [16]. Here, we aimed to affinity tag RdRp with two different tags to facilitate tandem affinity purification. We generated a recombinant replicon by introducing a His or HA tag into RdRp (aa sites: 25, 82, 442, or 483, respectively) of the RHDV replicon (Fig. 1A). Moreover, as predicated using the SWISS-MODEL online tool (https://swissmodel.expasy.org/), we found that insertion of the His and/or HA tag into these sites would have no effect on the structure of RdRp (Fig. S1). Fluc activity analysis showed that RHDV-luc-His_{25}, RHDV-luc-HA_{442}, and RHDV-luc-HA_{483} replicated similarly to the untagged RHDV replicon, whereas the replication ability of RHDV-luc-His_{82} was significantly inhibited in RK-13 cells (Fig. 1B). The same results were obtained in immunoblotting (IB) detection (Fig. 1C). The luciferase activity from the replicon lacking the RdRp gene has previously been shown to be approximately 4-logs lower than that of the wild type replicon [14]. In RHDV replicon, the viral sequence was generated as a consequence of polymerase II transcription from the cytomegalovirus (CMV) promoter, and the authentic 3' end of the viral genome was under controlled by a hepatitis delta virus ribozyme [17,18]. Subsequently, RdRp, VPg, and other non-structural proteins were translated in a cap-dependent manner by the host cell. The luciferase is expressed from the subgenomic RNA which generated by the RHDV RdRp. Thus, we could confirm insertion of His or HA tag at aa sites 25, 442 or 483 of RdRp.

Subsequently, we introduced HA and His peptides into RdRp simultaneously to obtain a double-affinity-tagged replicon (Fig. 1A). Fluc activity and IB analyses showed that RHDV-luc-His_{25}/HA_{442} and RHDV-luc-His_{25}/HA_{483} replicated similarly to the untagged RHDV replicon in RK-13 cells (Fig. 1D and 1E). Therefore, we used RHDV-luc-His_{25}/HA_{442} in affinity purification assays.

Identification of host factors associated with RHDV replicase

After transfection of RK-13 cells with the RHDV-luc-His_{25}/HA_{442} replicon for 48 h, solubilized cell lysates were sequentially purified using the HA and His tags. The untagged RHDV replicon acted as a negative control. After two-step affinity purification, the eluted protein complexes were resolved by sodium dodecyl sulfate polyacrylamide gel electrophoresis (SDS-PAGE) and the protein bands were visualized with silver staining (Fig. 2A). In total, 11 specific or enriched bands were sliced from the RHDV-luc-His_{25}/HA_{442} lane and the proteins they contained were identified using mass spectrometry (MS) (Table 1). The identified host proteins were associated with cytoskeleton components, intracellular transport, chaperone, RNP components, and translation machine-related proteins. Among these proteins, numerous proteins have been shown to interact with some single-stranded positive-strand RNA viral proteins to regulate viral replication, such as HnRNPK, HSPA8, DDX5, ANXA2, and PI4KA [19-23] (Fig. 2B and Table 1). In addition, the protein interaction network of the identified components of the RC was mapped using STRING online software (https://string-db.org/). As showed in Fig. 2C, there are intricate interaction networks for the components of the RHDV RC. We found that NCL not only binds to the RHDV replicase RdRp but it also interacts with many host proteins, such as casein kinase II subunit alpha (CSNK2A1), heterogeneous nuclear ribonucleoprotein K (HnRNPK), 40S ribosomal protein S5 (RPS5), 60S ribosomal protein L11 (RPL11), and so on.

168 **Table 1. Categories of host factors found to be associated with RHDV replicase[a]**

Category and band no.	Protein score	Mass (kDa)	Gene name	Protein description	No. of unique peptides	No. of peptides	SC (%)
RHDV protein							
6	273.3	57.8	*RdRp*	RHDV RdRp	3	4	21.1
10	186.4	25.1	*p23*	RHDV p23	2	3	15.5
11	165.8	16.2	*p16*	RHDV p16	2	4	10.4
Transport							
8	57.1	39.2	*ANXA2*	Annexin A2	4	7	10.4
1	201.3	233.6	*PI4KA*	Phosphatidylinositol 4-kinase alpha	6	6	30.5
5	303.5	68.9	*ALB*	Serum albumin	8	10	15.2
11	287.6	15.6	*HBA*	hemoglobin subunit alpha	5	5	40.4
6	173.2	59.7	*ATP5A1*	F-type H+-transporting ATPase subunit beta	3	3	7.8
11	365.6	16.1	*HBB*	hemoglobin subunit beta	7	9	58.7
9	98.3	32.9	*SLC25A5*	solute carrier family 25	3	3	11.2
11	99.8	12.6	*FABP5*	fatty acid-binding protein 5	3	4	13.5
Cytoskeleton							
11	105.5	14.3	*CFL1*	Cofilin 1	2	6	16.8
3	316.5	102.9	*ACTN1*	Actinin alpha 1	2	7	32.4
4	286.3	87.4	*ACTN4*	Actinin alpha 4	2	6	28.5
8	357.8	41.7	*ACTB*	Actin, cytoplasmic 1	2	5	19.0
7	419.4	53.6	*VIM*	Vimentin	13	13	25.3
RNP complex							
10	78.5	25.7	*HNRNPA1*	Heterogeneous nuclear ribonucleoprotein A1	3	7	13.6
10	67.9	30.3	*HNRNPAB*	Heterogeneous nuclear ribonucleoprotein A/B	2	6	8.9
7	127.2	50.9	*HNRNPK*	Heterogeneous nuclear ribonucleoprotein K	4	9	11.6
5	87.0	67.5	*DDX5*	DEAD-box helicase 5	2	4	8.3
5	90.6	69.4	*NCL*	Nucleolin	8	10	28.8
2	117.8	130.7	*SORBS2*	Sorbin and SH3 domain containing 2	5	5	14.7
10	135.6	26.2	*NUDT21*	cleavage and polyadenylation specificity factor subunit 5	3	3	10.4
5	99.1	70.9	*PABPC1*	Polyadenylate-binding protein 1	4	4	16.3
9	128.4	36.0	*YBX1*	Nuclease sensitive element-binding protein 1	5	6	22.1
6	112.1	57.4	*PTBP1*	Polypyrimidine tract-binding protein 1	4	7	6.7
6	65.2	52.1	*SRSF1*	splicing factor, arginine/serine-rich 1	6	7	8.8
5	75.9	63.5	*CPSF6*	cleavage and polyadenylation specificity factor subunit 6/7	3	10	10.9
6	75.2	62.5	*DDX41*	Probable ATP-dependent RNA helicase	3	12	14.5
Chaperon							
7	65.2	45.1	*CSNK2A1*	Casein kinase II subunit alpha	5	5	7.5
4	236.2	71.0	*HSPA8*	Heat shock cognate 71 kDa protein	7	7	14.2
9	153.9	30.7	*PYCR2*	Pyrroline-5-carboxylate reductase	4	5	16.8
3	70.1	116.8	*DSG1*	Desmoglein 1	2	5	9.0
11	50.3	14.7	*LYZ*	Lysozyme C	2	3	11.5
4	53.5	73.5	*HSPA9*	eat shock protein family A (Hsp70) member 9	2	2	13.8
10	152.2	26.2	*NUDT21*	Nudix hydrolase 21	3	3	24.5
8	142.8	40.3	*PDCD2L*	Programmed cell death protein 2-like	4	4	28.7
11	108.3	16.0	*FAM207A*	family with sequence similarity 207 member A	5	8	19.6

169 **Table1** (Continued)

Category and band no.	Protein score	Mass (kDa)	Gene name	Protein description	No. of unique peptides	No. of peptides	SC (%)
Translation machines							
7	94.2	50.0	*EEF1A*	Elongation factor 1-alpha	7	7	9.3
11	135.4	17.7	*RPS18*	Ribosomal protein S18	4	4	18.7
11	113.3	16.3	*AAES*	40S ribosomal protein S14	3	3	28.3
10	174.3	20.2	*RPL11*	Ribosomal protein L11	4	4	20.1
10	283.1	21.2	*RPL12*	Ribosomal protein L12	5	5	33.5
11	164.9	12.8	*RPL30*	60S ribosomal protein L30	4	4	50.5
11	68.3	15.5	*RPS17*	40S ribosomal protein S17	3	3	29.6
10	323.2	22.9	*RPS5*	Ribosomal protein S5	7	7	18.5
9	258.2	31.1	*RPS3*	40S ribosomal protein S3	9	9	25.8
7	74.4	45.3	*EIF4A1*	Eukaryotic initiation factor 4A-I	4	6	9.7
11	122.6	13.7	*RPS25*	Ribosomal protein S25	5	5	21.3
11	75.3	14.0	*RPS15A*	Ribosomal protein S15a	2	5	18.3

170 [a] Protein lists the gene name for each of the proteins identified in Fig.2B. SC refers to the percent sequence coverage for the
171 protein.
172

173 **NCL is involved in RHDV replication**

174 NCL is a phosphoprotein that is ubiquitously and abundantly expressed in many
175 eukaryotic cells and highly conserved during evolution, as it is involved in a remarkably large
176 number of cellular activities [24]. In general, NCL is mainly distributed in the nucleolus, but
177 it also exists in the nucleoplasm, cytoplasm, and cell surface, where its specific functions
178 vary, such as ribosome biogenesis, proliferation, and cell cycle regulation. NCL also plays
179 important roles in the replication and intracellular trafficking of multiple viruses [25-31].

180 To determine if NCL is required for RHDV replication, RK-13 cells were co-transfected
181 with an RHDV replicon, NCL siRNA or Flag-tagged NCL plasmids and internal control
182 plasmid encoding an *Rluc* gene. First, the effect of NCL siRNA on the viability of RK-13
183 cells was detected using a CCK-8 kit, according to the manufacturer's instruction. We found
184 that NCL knockdown would have some effect on cell viability and proliferation (Fig. S2A),
185 meanwhile, resulting the expression level of Rluc was affected (Fig. S2B). Since the toxicity,
186 cell number, and transfection efficiency of each treatment group have the same effect on the
187 RHDV replicon and Rluc plasmid, we used Rluc plasmids to eliminate the non-specific

effects of siRNA and other treatments on cells, and to correct the experimental data. The reporter luciferase activity was evaluated using a dual-luciferase reporter assay system with cell lysates that were harvested at 24 h and 48 h post-transfection (hpt). Fluc activity was normalized with respect to a co-transfected plasmid encoding an Rluc. Similar results were obtained in three independent experiments. The results showed that there is a positive correlation between the expression level of Fluc and NCL. This decreased with increasing NCL siRNA transfection dose and increased with increased dose of Flag-NCL transfection (Fig. 3A and 3B).

Subsequently, we examined the effect of NCL on mRHDV, which could proliferate in RK-13 cells [15]. We also used NCL siRNA or Flag-tagged NCL to change the expression level of NCL, and then infected with mRHDV (MOI = 1). At 48 hpi, the replication level of mRHDV were detected by WB and qPCR. The results were similar to RHDV replicons. As shown in Fig. 3C and 3D, the replication level of mRHDV increased with increased dose of Flag-NCL and decreased with increasing NCL siRNA.

In addition, we successfully constructed an RK-NCL cell line, which overexpressed the *NCL* gene, using a lentiviral packaging system (Fig. 3E). To evaluate the replication dynamics of mRHDV in RK-NCL cells, the cells were infected with mRHDV (MOI=1), and subsequently the expression level of VP60 was evaluated with qRT-PCR and WB at 48 hpi. The results showed that the expression level of VP60 in RK-NCL cells was significantly higher than that in control cells (RK-GFP cells and RK-13 cells) (Fig. 3E and 3F). Collectively, these data suggest that NCL is involved in RHDV replication.

NCL interaction with RHDV RdRp

NCL is a phosphoprotein with protein-binding activity, and it has been previously reported that NCL regulates viral replication by binding to viral proteins [32-40]. To

212 determine if NCL regulates RHDV replication through interaction with viral nonstructural
213 proteins, we used mammalian two-hybrid (M2H) assays to screen the interaction between
214 NCL and viral nonstructural proteins. As shown in Fig. 4A, NCL interacted with RdRp, p16,
215 and p23. To determine whether endogenous NCL binds to these viral nonstructural proteins,
216 during RHDV genome replication, we assessed the interaction between NCL and these viral
217 proteins in RK-13 cells, in the presence and absence of mRHDV infection for 24 h at 37 °C.
218 The results of an immunoprecipitation (IP) assay performed with cell lysates using NCL mAb
219 showed that regardless of whether the cell lysates were treated with RNase, NCL interacted
220 with RdRp, p16, and p23 in infected cells, but did not in uninfected cells (Fig. 4B).

221 RdRp is a replicase of RHDV that plays a key role in viral replication [41]. To prove
222 NCL interacts with RdRp, co-immunoprecipitation (Co-IP) assays were used with a myc
223 mAb in RK-13 cells, which were co-transfected with pRdRp-myc and pNCL-Flag eukaryotic
224 expression plasmids. We showed that overexpressed NCL-Flag was present in the anti-myc
225 (RdRp-myc) immunocomplex (Fig. 4C). Furthermore, NCL interacted with RdRp in RHDV-
226 infected cells (Fig. 4B). These results showed that NCL can interact with RHDV RdRp.
227 Moreover, an immunofluorescence assay (IFA) was performed using mAbs against NCL and
228 RdRp in RK-13 cells infected with mRHDV at 24 hours post infection (hpi). As shown in Fig.
229 4D, NCL was co-localized with RHDV RdRp in the RK-13 cell cytoplasm. In addition, the
230 distribution of NCL in the cytoplasm increased after RHDV infection.

231 The multifunctionality of NCL mainly results from its multidomain structure, which is
232 composed of three main structural domains: the N-terminal domain (NTD), the central
233 domain, and the C-terminal domain (CTD). The central domain contains fours RRMs, which
234 are also called RNA-binding domains (RBDs). To identify the functional domain of NCL for
235 NCL-RHDV RdRp interactions, GST fusion proteins corresponding to NCL and
236 subfragments (GST-NCL-NTD, GST-NCL-RBD, and GST-NCL-CTD, respectively) were

prepared for use as bait proteins in GST pull-down assays, to determine their abilities to interact with the RdRp protein expressed in RK-13 cells. As shown in Fig. 4E, GST-NCL and GST-NCL-RBD bound to RdRp whereas the other proteins were undetectable. This result confirmed that binding to RdRp requires the RBD domain of NCL. To further map the NCL RBD motif responsible for NCL-RdRp interactions, we prepared GST fusion proteins corresponding to subfragments of the NCL-RBD domain, including NCL-RRM1, NCL-RRM2, NCL-RRM3, and NCL-RRM4. A set of pull-down assays showed that GST-NCL-RBD and GST-NCL-RRM2 interact with RdRp whereas the other proteins did not (Fig. 4F). These findings indicate that NCL interacts with RHDV RdRp via the RRM2 motif.

To characterize the critical domain of RdRp for NCL-RdRp interactions, the GST fusion proteins corresponding to RdRp and subfragments of RdRp (GST-RdRp, GST-RdRp-N, GST-RdRp-M1, GST-RdRp-M2, GST-RdRp-M3, and GST-RdRp-C) were prepared for use as bait proteins in GST pull-down assays, to determine their ability to interact with the NCL protein expressed in RK-13 cells. The results of these assays showed that GST-RdRp, GST-RdRp-C and GST-RdRp-M2 bound to NCL, but the other proteins did not, and the binding ability of GST-RdRp-M2 to NCL is very weak (Fig. 4G). Subsequently, we prepared subfragments of $RdRp_{(341-516)}$ GST fusion proteins, including GST-$RdRp_{(341-493)}$, and GST-$RdRp_{(341-470)}$ for use as bait proteins in GST pull-down assays. As shown in Fig. 4H, GST-$RdRp_{(341-516)}$ and GST-$RdRp_{(341-493)}$ bound to NCL whereas GST-$RdRp_{(341-470)}$ did not. In addition, $RdRp_{(443-516)}$ was split into the fragments $RdRp_{(448-516)}$, $RdRp_{(453-516)}$, and $RdRp_{(458-516)}$; and $RdRp_{(341-493)}$ was split into the fragments $RdRp_{(341-485)}$, $RdRp_{(341-478)}$, and $RdRp_{(341-470)}$, which were fused with GST and expressed. The results of further pull-down assays showed that GST-$RdRp_{(443-516)}$, GST-$RdRp_{(448-516)}$, GST-$RdRp_{(341-493)}$, GST-$RdRp_{(341-485)}$, and GST-$RdRp_{(341-478)}$ bound to NCL whereas the other proteins did not (Fig. 4I). These results

suggest that NCL directly and specifically interacts with the C-terminal aa residues 448–478 of RHDV RdRp.

In addition, as predicated using the SWISS-MODEL online tool, we found that there is a "key" and "lock" structure formed by the amino acid sequence 448-478 of RdRp and RRM2 of NCL, providing space for the interaction between NCL and RdRp (Fig. 4J). Moreover, analysis of the RdRp sequence of GI.1a–GI.1d genotypes of RHDV showed that the C-terminal aa residues 448–478 were highly conserved (Fig. S3A). Together, these observations confirm that RHDV RdRp interacts with the RRM2 motif of NCL via the C-terminal aa residues 448–478, which is a conserved sequence in RHDV.

NCL interaction with RHDV p16

The function of p16 in RHDV remains unclear. Previous studies have reported that p16 can accumulate in subnuclear compartments, which may point to a specific interaction with nucleic acids and/or cellular proteins [42].

NCL is one of the most abundant proteins in the nucleolus. To investigate whether NCL directly interacts with p16, a Co-IP assay was performed with a myc mAb in RK-13 cells, which were co-transfected with p16-myc and NCL-Flag eukaryotic expression plasmids. IB analysis using a mAb against the Flag tag showed a band corresponding to NCL in the myc Co-IP assay, indicating a direct interaction between RHDV p16 and NCL (Fig. 5A). Moreover, we conducted an IFA using NCL mAbs and p16 polyclonal antibody in RK-13 cells infected with mRHDV at 24 hpi. As shown in Fig. 5B, NCL was co-localized with RHDV p16 in the RK-13 cell nucleolus and cytoplasm.

To investigate the functional areas of NCL in NCL-RHDV p16 interaction, the GST-NCL fusion protein and its subfragments were used as bait proteins in GST pull-down assays to

285 determine their ability to interact with the p16 protein. As shown in Fig. 5C, only GST-NCL
286 and GST-NCL-NTD bound p16. This result confirms that binding to p16 requires the NTD
287 domain of NCL. Subsequently, we prepared subfragments of NCL-NTD GST fusion proteins,
288 including NCL-NTD$_{(1-110)}$, NCL-NTD$_{(111-214)}$, and NCL-NTD$_{(215-318)}$ for use as bait proteins in
289 a set of GST pull-down assays. As shown in Fig. 5D, GST-NCL-NTD and GST-NCL-NTD$_{(1-}$
290 $_{110)}$ interact with p16 whereas the other proteins did not. Our data indicate that NCL interacts
291 with RHDV p16 via N-terminal residues 1–110.

292 Next, we identified the critical domain of p16 for NCL-p16 interactions using a series of
293 glutathione pull-down assays. First, the GST fusion proteins corresponding to p16 and
294 subfragments of p16 (GST-p16, GST-p16$_{(1-70)}$, GST-p16$_{(20-143)}$, GST-p16$_{(40-143)}$, GST-p16$_{(60-}$
295 $_{143)}$, and GST-p16$_{(70-143)}$) were prepared for use as bait proteins in GST pull-down assays, to
296 determine their ability to interact with NCL protein expressed in RK-13 cells. The results of
297 these assays showed that GST-p16, GST-p16$_{(1-70)}$ and GST-p16$_{(20-143)}$ bound to NCL, but the
298 other proteins did not (Fig. 5E-F). Subsequently, to pinpoint the key aa responsible for
299 binding of RHDV p16 with NCL, blocks of five aa substitutions were introduced within and
300 beyond the conserved sequence motif. The following non-conservative substitutions to the
301 GST-tagged RHDV p16 protein were made: ^{20}PLSFF^{24}TKVQQ, ^{25}LDLRD^{29}KRKHR,
302 ^{30}KTPPC^{34}LFATR, and ^{35}CIRAT^{39}RHDFP. Furthermore, GSGSGS was inserted after aa
303 residue 38. It has been reported that GSGSGS is a flexible peptide used in different
304 expression systems to separate functional proteins [43]. Wild-type and mutant RHDV p16
305 proteins were used as bait proteins in the GST pull-down assays to determine their ability to
306 bind NCL. As shown in Fig. 5G, the ^{35}CIRAT^{39}RHDFP mutation was not able to bind NCL;
307 the binding capacities of the other mutations to the residues at positions 20–40 were partially
308 reduced. In addition, analysis of the p16 sequence of the GI.1a–GI.1d genotypes of RHDV
309 showed that the ^{35}CIRAT^{39} motif was highly conserved (Fig. S3B). These observations

confirm that NCL interacts with RHDV p16 via aa residues 1–110 of the NTD domain of NCL bound to the ^{35}CIRAT^{39} motif of p16.

NCL interaction with RHDV p23

The function of p23 of RHDV is also unclear. Previous studies have reported that RHDV p23 is similar to other caliciviruses, which show an endoplasmic reticulum-like localization pattern [42]. It is well known that the murine norovirus (MNV), human norovirus (NV), and feline calicivirus (FCV) homologues of p23 play a role in the induction of intracellular membrane rearrangements associated with viral replication [44-46]. As previously described, NCL may have a direct role in the assembly of the ribosomal subunits by bringing together ribosomal proteins and RNA [47].

To identify whether p23 directly interacts with NCL, a Co-IP assay was used with a myc mAb in RK-13 cells, which were co-transfected with p23-myc and NCL-Flag eukaryotic expression plasmids. IB analysis using a mAb against the Flag tag showed a band corresponding to NCL in the myc Co-IP assay, indicating a direct interaction between RHDV p23 and NCL (Fig. 6A). In addition, we performed an IFA using mAbs against NCL and polyclonal antibody against p23 in RK-13 cells infected with mRHDV at 24 hpi. The result showed that NCL was co-localized with p23 in the RK-13 cell cytoplasm (Fig. 6B).

To characterize the critical domain of NCL for NCL-RHDV p23 interactions, the GST fusion proteins corresponding to NCL and subfragments were used as bait proteins in GST pull-down assays to determine their ability to interact with p23 protein expressed in RK-13 cells. As shown in Fig. 6C, both GST-NCL and GST-NCL-RBD bound to RHDV p23, but the other proteins did not. Subsequently, the subfragments of NCL-RBD GST fusion proteins were used as bait proteins in a GST pull-down assay. As shown in Fig. 6D, GST-NCL-RRM1 and GST-NCL-RBD bound to RHDV p23 whereas the other proteins did not. Together, these

results suggested that RHDV p23 directly and specifically interacts with RRM1 motif of NCL.

To map the RHDV p23 segments responsible for p23-NCL interactions, GST fusion proteins corresponding to subfragments of p23 ($p23_{(1-70)}$, $p23_{(70-145)}$, and $p23_{(145-224)}$) were prepared for use as bait proteins in GST pull-down assays to determine their ability to interact with NCL protein expressed in RK-13 cells. Results of a set of pull-down assays showed that GST-$p23_{(70-145)}$ and GST-p23 interact with NCL (Fig. 6E). Subsequently, subfragments of $p23_{(70-145)}$ GST fusion proteins including GST-$p23_{(90-145)}$, GST-$p23_{(110-145)}$, and GST-$p23_{(70-125)}$ were prepared for use as bait proteins in a GST pull-down assay. As shown in Fig. 6F, GST-$p23_{(90-145)}$ and $p23_{(70-145)}$ bound to NCL whereas the other proteins did not. Our data indicate that RHDV p23 interacts with NCL via aa residues 90–145. Moreover, as predicated using the SWISS-MODEL online tool, we found that there is a " mortise " and " tenon " structure formed by the amino acid sequence 90-145 of p23 and RRM1 of NCL, which providing a structural basis for the interaction between NCL and p23 (Fig. 6G). In addition, analysis of the p23 sequence of GI.1a–GI.1d genotypes of RHDV showed that the aa sequence 90–145 of RHDV p23 is conserved (Fig. S3C). These results suggest that NCL interacts with RHDV p23 via the RRM1 motif of NCL bound to the aa sequence 90–145 of p23.

NCL is required for RHDV replication

The above results fully demonstrated that NCL binds to the RdRp, p16, and p23 proteins of RHDV. To explore the role of these interactions in RHDV replication, a series of recombinant RHDV replicons were obtained by mutating or replacing the region that interacts with NCL in the wild-type RHDV replicon. The luciferase activity of RK-13 cells transfected with these recombinant RHDV replicons were analyzed and compared. The abundance of Fluc mRNA in the absence or presence of these binding sites, interacting with

NCL, was evaluated by qRT-PCR. Our results showed that the expression levels of Fluc derived from RHDV-luc/ΔRdRp, RHDV-luc/ΔRdRp$_{(448-478)}$, RHDV-luc/Δp16, RHDV-luc/Δp16$_{(35-38)}$, RHDV-luc/Δp23, and RHDV-luc/Δp23$_{(90-145)}$ were approximately 7%, 9%, 51%, 52%, 46%, and 44% respectively, compared with RHDV-luc (Fig. 7A). Subsequently, using the lentiviral packaging system, we successfully obtained RK-NCL-NTD, RK-NCL-RBD, and RK-NCL-CTD cell lines stably expressing the NCL NTD, RBD, and CTD domains, respectively (Fig. S4). We found that the replication levels of the RHDV replicon and mRHDV were significantly increased in RK-NCL and RK-NCL-RBD cells and significantly decreased in RK-NCL-NTD cells, but not in RK-NCL-CTD or RK-GFP cells (Fig. 7B and 7C). In addition, to better reflect the effects of NCL domains on RHDV replication, we inoculated mRHDV (MOI = 0.1) at low doses in each cell line. The mRHDV was constructed in our previous study and it has been determined that the virus can efficiently replicate in RK-13 cells [15]. The results showed that the level of replication of mRHDV in each cell line was similar to that of the RHDV replicon. From the above results, we revealed that the RBD domain is a functional domain that binds NCL to RdRp and p23, and the NTD domain is an active region that binds NCL to p16. Therefore, NCL segments that bind to the nonstructural proteins of RHDV play an important role in RHDV replication.

Moreover, we blocked the binding site of NCL-RdRp or NCL-p16 with a synthesized peptide (RdRp peptide: ERGVQLEELQVAAAAHGQEFFNFVRKELER; p16 peptide: PLSFFLDLRDKTPPCCIRAT, respectively) and examined the effect on the RHDV replicon and mRHDV replication. As shown in Fig. 7D and 7E, the replication level of the RHDV replicon and mRHDV were all drastically reduced in RK-13 cells treated with the RdRp peptides or p16 peptides, and there was a negative correlation with the dose of the synthesized peptide. Of course, the non-specific peptides (HKFGPVCLCNRAYIHDCGRW) had no effect on the replication of RHDV. We also found that these peptides have a greater

383 effect on the replication of RHDV replicon than mRHDV. Although the RHDV replicon is a
384 replication model of the virus, it lacks capsid protein and cannot be assembled into viral
385 particles. Therefore, the RHDV replicon may not fully reflect the replication process of the
386 virus in the cell. We speculate that there are some other mechanisms that regulate RHDV
387 replication.

388 In addition, the above experimental results were conducted using RK-13 cells infected
389 with mRHDV or transfected with the RHDV replicon. To assess the role of NCL-RdRp and
390 NCL-p16 interactions during infection with wild-type RHDV, rabbits were injected with the
391 RdRp peptide, p16 peptide, non-specific peptide or PBS, immediately after infection with
392 wild-type RHDV. Over the next 7 days, we counted deaths among experimental rabbits (Fig.
393 7F). As shown in Fig. 7G, the survival rates of rabbits against virulent RHDV in the groups
394 jnjected with RdRp peptide and p16 peptide was 60% and 40%, respectively. However, all
395 rabbits injected with in the non-specific peptide group and PBS group (negative controls)
396 died within 24–48 hpi with virulent RHDV. These negative control animals exhibited clinical
397 symptoms of RHDV infection.

398 Together, these results suggest that the interactions between NCL and the nonstructural
399 proteins of RHDV (RdRp, p16, and p23) have important roles in RHDV replication.
400 Importantly, NCL is required for RHDV replication.

401 **NCL is a link in RHDV replication complex (RC) formation**

402 The positive-strand RNA viruses share a conserved replication mechanism in which viral
403 proteins induce host membrane modification to assemble membrane-associated viral RCs
404 [12]. Viruses hijack host factors to facilitate this energy-unfavorable process [13]. Therefore,
405 the components of the viral RC are numerous and complex. NCL is capable of binding to

406 nonstructural proteins (RdRp, p16, and p23) of RHDV and is involved in the formation of
407 RHDV RCs.

408 To investigate the specific role of NCL in the formation of RHDV RCs, M2H assays were
409 used to screen the interactions between viral nonstructural proteins and multiple host factors
410 in RCs. As shown in Fig. 8A, there are complex interactions between viral nonstructural
411 proteins and host factors in RCs. For example, p16 interacts with itself, helicase, p29,
412 protease, and NCL; p23 binds to protease and NCL; p29 binds to helicase and VPg; helicase
413 interacts with itself; VPg binds to protease; protease interacts with itself and RPS5; RdRp
414 interacts with RPS5; and NCL binds to HnRNPK, CSNK2A1, RPS5, and RPL11. We
415 subsequently used a series of Co-IP assays with a myc mAb in RK-13 cells, which were co-
416 transfected with bait (myc fusion protein) and prey (Flag fusion protein) eukaryotic
417 expression plasmids. IB analysis using a mAb against Flag showed the specific band
418 corresponding to prey proteins in the myc Co-IP assay (Fig. 8B). These results reveal that
419 RHDV replicase RdRp cannot directly bind to other nonstructural proteins of the virus. It is
420 noteworthy that NCL directly interacts with RHDV RdRp and nonstructural proteins (p16
421 and p23).

422 To test the hypothesis that nucleolin acts as a platform for the RdRp to be attracted to the
423 p16 and p23 proteins, a series of HA tag affinity purification analyses were performed by
424 transfection with the RHDV-luc-His/HA replicon in RK-13 cells that were treated with RdRp
425 peptide, NCL siRNA, or PBS, and in RK-NCL cells. Using IB to detect the purified RdRp-
426 associated protein, we found that the content of purified p16 and p23 in the RdRp peptide- or
427 NCL siRNA-treated cells was significantly reduced or even lost in the RC, and partially
428 increased in RK-NCL cells (Fig. 8C). In addition, the eluted protein complexes were resolved
429 by SDS-PAGE and the protein bands were visualized with silver staining. As shown in Fig.
430 8D, the RdRp-associated protein content was significantly reduced in RdRp peptide- or NCL

siRNA-treated cells and significantly increased in RK-NCL cells.Together, these data suggest that RHDV completes its replication process by hijacking NCL to recruit other viral proteins and host factors, to thus assemble the RHDV RC.

Discussion

Positive-strand RNA viruses encompass more than one-third of known virus genera and include many medically and practically important human, animal, and plant pathogens [48]. At the outset of infection, positive-strand RNA virus genomes are used as templates for viral protein synthesis in cytoplasm. Subsequently, viral protein recruits host factors to form an RC and redirects the viral genome to function as mRNA, serving as a template for synthesizing new positive-strand gRNA and subgenomic mRNA [48]. Therefore, identification of the components of the viral RC and the interrelationships among the various components, particularly those that interact with viral replicase, will help in understanding the molecular mechanisms of viral replication.

As an important member of the positive-strand RNA viruses, the *Caliciviridae* family has attracted increasing attention because it contains many viruses that infect a wide spectrum of hosts and are a growing threat to human and animal health. However, most caliciviruses cannot be cultured *in vitro*, including some important pathogens such as RHDV and NV; therefore, the replication and pathogenic mechanisms of these viruses remain poorly understood. The emergence and advancement of reverse genetic manipulation technology has provided an excellent operating platform for revealing the molecular mechanism of calicivirus replication. For example, using a NV replicon, a series of works have been carried out to reveal the mechanism of NV replication [49-53]. Recently, we also successfully established an RHDV replicon operating platform [14] and have applied it to study the genomic structure and function of RHDV.

In this study, we purified viral replicase and identified the replicase-associated host factors using an RHDV replicon system in which two different affinity tags were simultaneously inserted in-frame into RdRp. We determined that NCL plays a key role in the formation of RHDV RCs. On the one hand, NCL binds to RHDV replicase (RdRp) (Fig. 4). Similar to other positive-sense RNA viruses, RHDV RdRp has a central role in the viral replication cycle. RdRp has many enzymatic properties; it binds template RNAs, initiates replication, catalyzes elongation, and terminates replication [54]. Moreover, RdRp is able to induce the redistribution of Golgi membranes in kidney and liver cell lines of three different species [55]. Here, our data suggested that interaction between NCL and RdRp is required for RHDV replication (Fig. 7). On the other hand, NCL also interacts with some important host factors, such as HNRNPK, RPL11, CSNK2A1, and RPS5 (Figs. 2, 8, 9). Previous studies have shown that these proteins are involved in the replication of various viruses. For example, HNRNPK has been reported to recognize the 5' terminal sequence of HCV RNA [56], CSNK2A1 interaction with NS1 plays an important part in parvovirus replication [57]; and RPL11 and RPS5 are components of the ribonucleoprotein complex [58,59]. Therefore, we hypothesize that these host factors may also be involved in the replication of RHDV.

We also identified that NCL interacts with nonstructural proteins (p16 and p23) of RHDV (Figs. 5, 6). By blocking the interaction of NCL with p16 and p23, we found that these interactions have important roles in RHDV replication (Fig. 7). Previous studies have reported that p16 can accumulate in subnuclear compartments, which may point to a specific interaction with nucleic acids and/or cellular proteins [42]. A similar nuclear/subnuclear accumulation of nonstructural proteins has been reported in picornavirus, for which nuclear accumulation of the 2A protein and a close association of this protein with the nucleolar ribosomal chaperone protein B23 have been reported. It was suggested that 2A upregulates the formation of modified ribosomes with a preference for viral internal ribosomal entry sites,

480 thereby contributing to the inhibition of cap-dependent cellular mRNA translation [60]. Here,
481 we revealed that NCL interacts with p16 of RHDV via the NTD domain (Fig. 5) and that this
482 interaction plays a role in RHDV replication (Fig. 7). The N-terminal domain of NCL
483 contains acidic regions, rich in glutamic acid and aspartic acid, which are the sites of
484 phosphorylation and participate in the transcription of rRNA and interact with components of
485 the pre-rRNA processing complex [24]. Therefore, we speculate that RHDV utilizes the
486 interaction between p16 and NCL to hijack NCL-associated machinery of rRNA transcription
487 and pre-rRNA processing to replicate viral gRNA. In addition, the role of p23 in RHDV
488 replication is still unclear. Previous studies have found that, similar to other caliciviruses,
489 RHDV p23 is enriched in the endoplasmic reticulum membrane and plays an important part
490 in inducing intracellular membrane rearrangement [42]. Therefore, we believe that p23
491 interacts with NCL to recruit replication-associated host proteins to the endoplasmic
492 reticulum membrane, and assembles these to form membrane-associated RCs.

493 NCL is an abundant and ubiquitously expressed protein in many growing eukaryotic cells
494 [24]. NCL is mainly localized within the nucleolus, but it also exists in the nucleoplasm,
495 cytoplasm, and cell surface [25,26]. NCL controls a wide range of fundamental cellular
496 processes, such as ribosome biogenesis, proliferation, and cell cycle regulation, and it also
497 has important roles in the infection process of multiple viruses [24]. For example, NCL acts
498 as a receptor for human respiratory syncytial virus [61]. NCL also mediates cellular
499 attachment and internalization of enterovirus 71 [62]. A recent study showed that NCL
500 interacts with the capsid protein of dengue virus, suggesting a role in viral morphogenesis
501 [63]. In previous studies, we also found that NCL mediates the internalization of RHDV
502 through interacting with the RHDV capsid protein [64]. Of note, NCL also plays an important
503 part in replication of several viruses. For example, NCL interacts with the FCV NS6
504 (protease) and NS7 (polymerase) proteins, and has a role in virus replication [34]. Similarly,

505 the interaction between NCL and the UTRs of FCV [34] and poliovirus [65] stimulates
506 translation of viral proteins. Moreover, NCL binds to a protein of herpes simplex virus type 1
507 to facilitate the export of US11 from the cell nucleus to the cytoplasm [66]. However, the
508 function of NCL in binding to RHDV replicase and recruiting host factors to form RCs had
509 not been revealed until now. Here, we demonstrate for the first time that NCL can
510 specifically bind to RHDV replicase (RdRp) and can act as a link, recruiting host factors and
511 viral proteins, to form RHDV RCs. Our findings enrich the current knowledge about the
512 mechanism of NCL regulation of viral replication and provides new clues for further
513 exploration of the interaction between RHDV and host proteins.

514 In conclusion, we identified the components of the RHDV RC, for the first time. We
515 found that NCL acts as a link to recruit host factors, viral replicase (RdRp), and nonstructural
516 proteins (p16 and p23), thereby forming a complex and ordered RHDV RC (Fig. 9).
517 Elucidation of the molecular mechanism by which NCL regulates viral replicase assembly
518 may lead to new insights into viral RC biogenesis and novel antiviral strategies.

519 ## Materials and Methods

520 ### Ethics Statement

521 All experiments were performed in a secondary biosecurity laboratory. All experiments
522 involving rabbits were carried out in strict accordance with the recommendations of the
523 Guide for the Care and Use of Laboratory Animals of the Ministry of Science and
524 Technology of the People's Republic of China, and all efforts were made to minimize
525 suffering. All animal procedures were approved by the Institutional Animal Care and Use
526 Committee of the Shanghai Veterinary Research Institute, Chinese Academy of Agricultural
527 Sciences (permit number: SHVRIAU-18-035).

528 ### Plasmids

The pRHDV-luc plasmid, in which the *VP60* and partial *VP10* genes are replaced with the *Fluc* gene, was generated in our previous study [14]. To generate pRHDV-luc-HA1, pRHDV-luc-HA2, pRHDV-luc-His1, and pRHDV-luc-His2, the nucleotide sequence encoding a hemagglutinin (HA) peptide (TAC CCA TAC GAT GTT CCA GAT TAC GCT) or a His_6 peptide (CAT CAT CAT CAT CAT CAT) were inserted into the RdRp region using fusion polymerase chain reaction (PCR). The pRHDV-luc-His1/HA1, pRHDV-luc-His1/HA2, pRHDV-luc-His2/HA1, and pRHDV-luc-His2/HA2 plasmids, in which HA and His tags were simultaneously inserted in-frame into RdRp, were generated by fusion PCR (Fig. 1A). In addition, pRHDVΔp16-luc, pRHDVp16(^{35}RHDF^{38})-luc, pRHDVΔp23-luc, pRHDVΔp23(90-145)-luc, pRHDVΔRdRp-luc, and pRHDVΔRdRp(448-478)-luc were constructed using fusion PCR.

The lentivirus-based expression plasmids were generated with a pLOV-CMV-GFP vector (Neuron Biotech, China) using In-Fusion HD Cloning kits (Clontech Laboratories, Inc., USA), according to the manufacturer's instructions. The pLOV-CMV-GFP vector was linearized with N*he* I and N*ot* I. The packaging plasmid psPAX2 containing the specific lentivirus genes Gag, Pol, and so on, and the pMD2.G plasmid, which expresses the G protein of the vesicular stomatitis virus (VSV-G), were purchased from Neuron Biotech.

The plasmids, used in M2H assays, were generated with the pACT and pBIND vectors (Promega Corporation, USA) using In-Fusion HD Cloning kits. The pG5luc vector (Promega) contains five GAL4 binding sites upstream of the TATA box, which controls *Fluc* expression. The pGL4.75 vector (Promega) encodes the luciferase reporter gene *Renilla reniformis* (*Rluc*) from a CMV promoter.

The p3×FLAG-CMV-14 vector (Sigma-Aldrich Corporation, USA) and pCMV-Myc (Clontech Laboratories, Inc.) were used to create mammalian expression constructs. The pGEX-4T-1 vector (GE Healthcare Life Sciences, USA) was expressed in competent *E. coli*

554 BL21-CodonPlus (DE3) cells. *NCL* (GenBank accession number XM_017343189.1),
555 *CSNK2A1* (GenBank accession number NM_001160284.1), *HnRNPK* (GenBank accession
556 number NM_001082125.1), *RPL11* (GenBank accession number XM_008265690.2), and
557 *RPS5* (GenBank accession number XM_002721896.3) sequences were amplified by reverse
558 transcription PCR (RT-PCR) from an RK-13 cell cDNA library. Total RNA was isolated
559 from RK-13 cells using TRIzol reagent (Invitrogen Corporation, USA), according to the
560 manufacturer's instructions. DNA was removed from the isolated RNA using DNase I
561 (Takara Bio, Inc., Japan) and cDNA was produced with Moloney murine leukemia virus
562 reverse transcriptase (M-MLV RT) (Promega) and random hexamers. RHDV genes (*p16, p23,*
563 *helicase, p29, VPg, protease*, and *RdRp*) were amplified using RT-PCR from RHDV cDNA.
564 The genomic sequence of RHDV CHA/JX/97 was retrieved from the GenBank database
565 (accession number DQ205345). Viral cDNA was generated as described in our previous
566 report. All plasmids were created using In-Fusion HD Cloning kits, according to the
567 manufacturer’s instructions.

568 All RT-PCR and PCR amplifications for cloning were performed with TransStart®
569 FastPfu Fly DNA Polymerase (TransGen Biotech Co., Ltd., China), according to the
570 manufacturer’s instructions. RT-PCR and PCR products were separated by agarose gel
571 electrophoresis and purified with a SanPrep Column DNA Gel Extraction Kit (Sangon
572 Biotech Co., Ltd., China). Restriction digests were performed using commercial kits (New
573 England Biolabs, USA), according to the manufacturer’s instructions. All plasmid sequences
574 were amplified by PCR and analyzed by Sanger sequencing, to verify the sequence fidelity
575 and reading frames (Sangon Biotech). The details of all constructs used in the study,
576 including residue numbers, expression vectors, and tags, are summarized in Table S1. In
577 addition, the primers used in this research are listed in Table S2.

578 **Cell lines and viruses**

Rabbit kidney cells (RK-13, ATCC, CCL37) and 293T cells (ATCC, CRL-3216) were routinely maintained in minimal essential medium (MEM) (Life Technologies, USA) or Dulbecco's modified Eagle's medium (DMEM) (Life Technologies), respectively, supplemented with 10% fetal bovine serum (Biological Industries, Israel). RK-NCL cells, RK-NCL-NTD cells, RK-NCL-RBD cells, RK-NCL-CTD cells, and RK-GFP cells were generated by transducing RK-13 cells with VSV-G pseudotyped lentiviral particles, which contain the *NCL* gene, NCL-NTD domain, NCL-RBD domain, NCL-CTD domain, or *GFP* gene. To generate those recombinant lentiviral particles, we transfected psPAX2 (10 μg), pMD2.G (12 μg), and pLOV-NCL-GFP (22 μg), pLOV-NTD-GFP (22 μg), pLOV-RBD-GFP (22 μg), pLOV-CTD-GFP (22 μg) or pLOV-CMV-GFP (22 μg), respectively, into 293T cells, which were seeded (1×10^6 cells) onto 100-mm tissue culture dishes, using a calcium phosphate transfection reagent (Invitrogen). The lentivirus packaging and transduction procedures are based on our previous studies [4]. For the RHDV replicon replication assay, these five stable cell lines, with exactly the same number of passages, were used to avoid the effect of cell passage variation on RHDV replication.

RHDV strain JX/CHA/97 was isolated in 1997 during an outbreak of RHDV in China and stored in our laboratory. The genomic sequence of RHDV CHA/JX/97 is available in the GenBank database (accession number DQ205345). mRHDV was mutated from RHDV strain JX/CHA/97 and stored in our laboratory [15].

Antibodies and chemicals

The antibodies used in this study included: mouse anti-His, anti-HA, anti-luc, and anti-myc antibodies purchased from Abcam; mouse anti-Flag obtained from Sigma-Aldrich; mouse anti-β-actin and anti-GST antibodies purchased from Kangwei Century Biotechnology; mouse anti-NCL and rabbit anti-NCL obtained from Thermo Fisher Scientific; mouse anti-

603 RHDV RdRp was prepared by Genscript and stored in our laboratory; polyclonal rabbit anti-
604 RHDV p16 and anti- RHDV p23 were prepared and stored in our laboratory; goat anti-
605 mouse IgG conjugated with HRP and goat anti-rabbit IgG conjugated with HRP purchased
606 from Jackson ImmunoResearch Europe Ltd.; goat anti-mouse IgG conjugated with Alexa
607 Fluor 488, goat anti-rabbit IgG conjugated with Alexa Fluor 488, goat anti-mouse IgG
608 conjugated with Alexa Fluor 633, and goat anti-rabbit IgG conjugated with Alexa Fluor 633,
609 obtained from Thermo Fisher Scientific. DAPI staining solution purchased from Beyotime
610 Biotechnology. N*he* I and N*ot* I obtained from New England Biolabs. CCK-8 kit purchased
611 from Dojindo Laboratories. RdRp peptide
612 (ERGVQLEELQVAAAAHGQEFFNFVRKELER), p16 peptide
613 (PLSFFLDLRDKTPPCCIRAT) and non-specific peptide (HKFGPVCLCNRAYIHDCGRW)
614 were synthesized by GL Biochem (Shanghai) Ltd, and the purity was 90%. We dissolved
615 these peptides in PBS at a concentration of 10 ng/μL. Then, these peptides were directly
616 added into the cell culture medium at different working concentrations, respectively, and
617 these peptides entered in the cytoplasm by macropinocytosis.

618 **Affinity purification of protein complex**

619 RK-13 cells were seeded onto ten 100-mm tissue culture dishes at a density of 1×10^6
620 cells/dish. The cells were grown overnight and then transfected with pRHDV-luc-His1/HA1
621 (12 μg /dish) using Lipofectamine 3000 (Invitrogen), according to the manufacturer's
622 instructions. After 48 hpt, the cells were washed three times with cold Modified Dulbecco's
623 phosphate-buffered saline (MDPBS; Thermo Scientific™ Pierce™, USA). The cells were
624 then lysed with 500 μL/dish of ice-cold lysis buffer (Tris, 0.15 M NaCl, 0.001 M EDTA, 1%
625 NP-40, 5% glycerol; pH 7.4, proteinase inhibitor cocktail (Thermo Scientific). After
626 incubating cells on ice for 5 min with periodic mixing, the lysate was transferred to a

microcentrifuge tube and centrifuged at ~ 13,000 × g for 10 min to pellet the cell debris. The soluble fraction was incubated by head-to-tail rotation with 300 µL of anti-HA antibody-coated beads (Thermo Scientific) for 4 h at 4°C. The beads were collected by centrifugation and then washed four times with 10 mL washing buffer (Tris, 0.15 M NaCl, 0.001 M EDTA, 1% NP-40, 5% glycerol; pH 7.4, 20 mM imidazole (Thermo Scientific). After being washed, the bound proteins were eluted with 400 µL of wash buffer supplemented with 250 µg/mL HA peptide (Sigma-Aldrich) by incubation at room temperature for 10 min. After centrifugation at 3,000 × g for 5 min, followed by a second elution with 200 µL of wash buffer supplemented with 250 µg/mL HA peptide. The eluted solutions were combined and diluted into 1.5 mL of lysis buffer containing 20 mM imidazole, and 60 µL of Ni Sepharose (Thermo Scientific) was added. After incubation at 4°C for 1 h and clarification, the beads were washed four times with 1.5 mL wash buffer. The captured proteins were eluted in 80 µL wash buffer containing 240 mM imidazole and mixed with 20 µL of 5X SDS loading buffer (250 mM Tris Cl (pH 6.8), 30% glycerol, 10% SDS, 0.02% bromophenol blue, 25% 2-mercaptoethanol). After being boiled for 10 min, the proteins samples were separated by SDS-PAGE, and protein bands were visualized with silver staining.

Quantitative reverse transcription (qRT)-PCR

Total RNAs were purified using TRIzol reagent (Invitrogen), according to the manufacturer's instructions. DNA was removed from the isolated RNA using DNase I (Takara), and then cDNA was produced using M-MLV RT (Promega) and random hexamers. The cDNA samples were subjected to real-time PCR with SYBR Premix *Ex Taq* Tli RNase H Plus (Takara) using an ABI 7500 Fast Real-Time PCR system (Applied Biosystems, USA). The primers are listed in Table S2. The relative RNA levels were determined according to the $2^{-\Delta\Delta CT}$ method. The amount of mRNA in each sample was normalized to that of GAPDH.

651 **Mammalian two-hybrid (M2H) assays**

652 The interactions between host protein and RHDV nonstructural proteins were evaluated
653 using a CheckMate Mammalian Two-Hybrid System (Promega). The proteins expressed
654 from the pACT vector recombinant plasmid acted as prey proteins, and proteins expressed
655 from the pBIND vector recombinant plasmid acted as bait proteins. Subsequent M2H
656 analysis was performed, according to the manufacturer's instructions. In brief, bait and prey
657 plasmids were co-transfected with pG5luc plasmids into subconfluent 293T cells at a molar
658 ratio of 1:1:1 for pACT: pBIND: pG5luc vector. At 48 h after transfection, the 293T cells
659 were lysed, and Renilla luciferase (Rluc) and firefly luciferase (Fluc) activities were
660 evaluated using the Dual-Luciferase Reporter (DLR™) Assay System (Promega).

661 **Luciferase activity measurements**

662 Cells were washed with PBS and lysed in 200 μL of 1X Passive Lysis Buffer (Promega).
663 After gentle shaking for 15 min at room temperature, the cell lysate was transferred to a tube
664 and centrifuged for 2 min at 12,000 × g at 4ºC. The supernatant (20 μL) was added to 100 μL
665 of luciferase assay substrate to evaluate the activity of Fluc and Rluc using the Promega
666 DLR™ assay system, based on relative light units (RLUs). Luciferase activity was analyzed
667 using a FB12 luminometer (Berthold, Germany). To normalize the luciferase values
668 determined for cells transfected with the Fluc replicon, Rluc activity was used as an internal
669 control.

670 **Bacterial expression of recombinant proteins and purification**

671 All proteins were expressed in competent *E. coli* BL21-CodonPlus (DE3) cells (TransGen
672 Biotech Co., Ltd.) that were seeded in 1 mL of an overnight starter culture and then grown in
673 100 mL of Luria-Bertani (LB) broth with shaking at 220 rpm at 37°C to mid-log phase

(~0.6–0.8 OD_{600}). Cells were then typically induced with 0.2–0.5 mM isopropyl β-D-1-thiogalactopyranoside and incubated for approximately 16 h at 16°C with shaking at 220 rpm. The details of protein expression are available on request. Cells were pelleted by centrifugation at ~5,000 × g and stored at −80°C. Bacterial pellets were resuspended in lysis buffer (20 mM Tris/HCl; pH 7.4, 60 mM NaCl, 1 mM ethylenediaminetetraacetic acid (EDTA), 1 mg/mL lysozyme, 1 mM dithiothreitol, and 0.1% Triton X-100) supplemented with complete protease inhibitor cocktail (Thermo Scientific) for 1 h on ice. Nuclease was then added and the lysate was incubated for 1 h at ambient temperature under rotation. The lysates were centrifuged at 4°C for 10 min at 12,000 × g. Glutathione Sepharose 4B beads (Pierce Biotechnology, USA) were added to the clarified supernatants and the mixtures were incubated overnight at 4°C under rotation. The beads were washed with lysis buffer, followed by three washes with PBS, and then stored at 4°C in an equal volume of PBS.

Glutathione-S-transferase (GST) pull-down assay

For the *in vitro* binding assay, Flag- or myc-tagged NCL, and RHDV p16, p23, and RdRp proteins were expressed in RK-13 cells. According to the manufacturer's instructions, the GST pull-down assay was performed by incubating 50 µL of a 50% slurry of glutathione Sepharose beads containing 25 µM GST fusion protein in lysis buffer with a 3-fold molar excess of prey protein (Pierce Biotechnology). RNase (Takara) was added to the cell lysis and wash buffers. The bound proteins were separated by SDS-PAGE and then subjected to western blot analysis.

Co-immunoprecipitation (Co-IP) analysis

RK-13 cells were co-transfected with the bait and prey plasmids. At 48 h after transfection, total protein was isolated from RK-13 cells using IP lysis buffer. We conducted Co-IP analysis using a commercial Co-IP kit (Pierce Biotechnology), according to the

manufacturer's instructions. AminoLink Plus Coupling Resin (Thermo Scientific) was incubated with anti-myc monoclonal antibody (mAb) (Abcam, UK) or anti-Flag mAb (Abcam) and then subjected to SDS-PAGE. IB analysis of the proteins was subsequently conducted using mAbs against myc and Flag (Abcam). RNase was added to the cell lysis and wash buffers.

Immunoblotting (IB) analysis

Protein samples were separated on 12% gels and then transferred to nitrocellulose membranes (Hybond-C; Amersham Life Sciences, UK) using a semi-dry transfer apparatus (Bio-Rad Laboratories, USA). The membranes were blocked with 5% (w/v) nonfat milk in TBST buffer (150 mM NaCl, 20 mM Tris, and 0.1% Tween-20; pH 7.6) for 3 h at 4°C and then stained overnight at 4°C with a primary antibody (Ab). After washing three times for 10 min each, the membranes were incubated with a secondary Ab against immunoglobulin G (IgG) conjugated to horseradish peroxidase (Sigma-Aldrich) in PBST buffer (137 mM NaCl, 2.7 mM KCl, 10 mM Na_2HPO_4, 2 mM KH_2PO_4 and 0.1% Tween-20; pH 7.4) for 1 h at room temperature (RT). Finally, after washing three times for 10 min each, the proteins were detected using an automatic chemiluminescence imaging analysis system (Tanon Science & Technology Co., Ltd., China).

Immunofluorescence assay (IFA)

Cells were fixed in 3.7% paraformaldehyde in PBS (pH 7.5) at RT for 30 min and subsequently permeabilized by incubation in methanol at −20°C for 30 min. The fixed cells were blocked with 5% (w/v) nonfat milk in PBST buffer for 3 h at 4°C and then stained with a primary Ab for 2 h at 37°C. After washing three times for 10 min each, the cells were incubated with a secondary Ab against IgG conjugated to fluorescein isothiocyanate (FITC) (Sigma-Aldrich) in PBST buffer for 1 h at room temperature. Finally, after washing three

times for 10 min each, the samples were observed under a fluorescence microscope equipped with a video documentation system (ZEISS, Germany).

Mass spectrometry

Jingjie PTM BioLab Co., Ltd. (Hangzhou, China) performed all mass spectrometry analyses.

In vivo experiments

Twenty 8-week-old male New Zealand rabbits seronegative for RHDV were randomly distributed into four groups (n = 5/group) and housed in individual ventilated cages. All experimental protocols were reviewed by the state ethics commission and were approved by the competent authority. Details of the protection assay are shown in Fig. 7F. All rabbits were challenged intramuscularly with 100 × the median lethal dose (LD50) of RHDV. Two hours after RHDV infection, rabbits were injected with the RdRp peptide (1 mg), p16 peptide (1 mg), non-specific peptide (1 mg), or PBS, via the ear vein. The rabbits were clinically examined daily for 7 days post-challenge.

Statistical analyses

Statistical analysis was performed using GraphPad Prism 6 software. Specific tests are described in the figure legends.

Acknowledgments

We thank LetPub for its linguistic assistance during the preparation of this manuscript.

References

1. Meyers G, Wirblich C, Thiel HJ (1991) Rabbit hemorrhagic disease virus--molecular cloning and nucleotide sequencing of a calicivirus genome. Virology 184: 664-676.
2. Gregg DA, House C, Meyer R, Berninger M (1991) Viral haemorrhagic disease of rabbits in Mexico: epidemiology and viral characterization. Rev Sci Tech 10: 435-451.
3. Abrantes J, van der Loo W, Le Pendu J, Esteves PJ (2012) Rabbit haemorrhagic disease (RHD) and rabbit haemorrhagic disease virus (RHDV): a review. Vet Res 43: 12.
4. Zhu J, Miao Q, Tan Y, Guo H, Li C, et al. (2016) Extensive characterization of a lentiviral-derived stable cell line expressing rabbit hemorrhagic disease virus VPg protein. J Virol Methods 237: 86-91.
5. Zhu J, Wang B, Miao Q, Tan Y, Li C, et al. (2015) Viral Genome-Linked Protein (VPg) Is Essential for Translation Initiation of Rabbit Hemorrhagic Disease Virus (RHDV). PLoS One 10: e0143467.
6. Meyers G, Wirblich C, Thiel HJ (1991) Genomic and subgenomic RNAs of rabbit hemorrhagic disease virus are both protein-linked and packaged into particles. Virology 184: 677-686.
7. Wirblich C, Sibilia M, Boniotti MB, Rossi C, Thiel HJ, et al. (1995) 3C-like protease of rabbit hemorrhagic disease virus: identification of cleavage sites in the ORF1 polyprotein and analysis of cleavage specificity. J Virol 69: 7159-7168.
8. Morales M, Barcena J, Ramirez MA, Boga JA, Parra F, et al. (2004) Synthesis in vitro of rabbit hemorrhagic disease virus subgenomic RNA by internal initiation on (-)sense genomic RNA: mapping of a subgenomic promoter. J Biol Chem 279: 17013-17018.
9. Meyers G (2003) Translation of the minor capsid protein of a calicivirus is initiated by a novel termination-dependent reinitiation mechanism. J Biol Chem 278: 34051-34060.
10. Marin MS, Casais R, Alonso JM, Parra F (2000) ATP binding and ATPase activities associated with recombinant rabbit hemorrhagic disease virus 2C-like polypeptide. J Virol 74: 10846-10851.
11. Lopez Vazquez AL, Martin Alonso JM, Parra F (2001) Characterisation of the RNA-dependent RNA polymerase from Rabbit hemorrhagic disease virus produced in Escherichia coli. Arch Virol 146: 59-69.
12. den Boon JA, Ahlquist P (2010) Organelle-like membrane compartmentalization of positive-strand RNA virus replication factories. Annu Rev Microbiol 64: 241-256.
13. Nagy PD, Pogany J (2011) The dependence of viral RNA replication on co-opted host factors. Nat Rev Microbiol 10: 137-149.
14. Wang B, Zhe M, Chen Z, Li C, Meng C, et al. (2013) Construction and applications of rabbit hemorrhagic disease virus replicon. PLoS One 8: e60316.
15. Zhu J, Miao Q, Tan Y, Guo H, Liu T, et al. (2017) Inclusion of an Arg-Gly-Asp receptor-recognition motif into the capsid protein of rabbit hemorrhagic disease virus enables culture of the virus in vitro. J Biol Chem 292: 8605-8615.
16. Yi Z, Fang C, Zou J, Xu J, Song W, et al. (2016) Affinity Purification of the Hepatitis C Virus Replicase Identifies Valosin-Containing Protein, a Member of the ATPases Associated with Diverse Cellular Activities Family, as an Active Virus Replication Modulator. J Virol 90: 9953-9966.
17. Kümmerer BM (2018) Establishment and Application of Flavivirus Replicons. In: Hilgenfeld R, Vasudevan SG, editors. Dengue and Zika: Control and Antiviral Treatment Strategies. Singapore: Springer Singapore. pp. 165-173.
18. Khromykh AA, Varnavski AN, Sedlak PL, Westaway EG (2001) Coupling between replication and packaging of flavivirus RNA: evidence derived from the use of DNA-based full-length cDNA clones of Kunjin virus. J Virol 75: 4633-4640.

19. Hsieh TY, Matsumoto M, Chou HC, Schneider R, Hwang SB, et al. (1998) Hepatitis C virus core protein interacts with heterogeneous nuclear ribonucleoprotein K. J Biol Chem 273: 17651-17659.
20. Saxena V, Lai CK, Chao TC, Jeng KS, Lai MM (2012) Annexin A2 is involved in the formation of hepatitis C virus replication complex on the lipid raft. J Virol 86: 4139-4150.
21. Kovalev N, Nagy PD (2014) The expanding functions of cellular helicases: the tombusvirus RNA replication enhancer co-opts the plant eIF4AIII-like AtRH2 and the DDX5-like AtRH5 DEAD-box RNA helicases to promote viral asymmetric RNA replication. PLoS Pathog 10: e1004051.
22. Zhang C, He L, Kang K, Chen H, Xu L, et al. (2014) Screening of cellular proteins that interact with the classical swine fever virus non-structural protein 5A by yeast two-hybrid analysis. J Biosci 39: 63-74.
23. Dorobantu CM, Albulescu L, Harak C, Feng Q, van Kampen M, et al. (2015) Modulation of the Host Lipid Landscape to Promote RNA Virus Replication: The Picornavirus Encephalomyocarditis Virus Converges on the Pathway Used by Hepatitis C Virus. PLoS Pathog 11: e1005185.
24. Jia W, Yao Z, Zhao J, Guan Q, Gao L (2017) New perspectives of physiological and pathological functions of nucleolin (NCL). Life Sci 186: 1-10.
25. Tuteja R, Tuteja N (1998) Nucleolin: a multifunctional major nucleolar phosphoprotein. Crit Rev Biochem Mol Biol 33: 407-436.
26. Abdelmohsen K, Gorospe M (2012) RNA-binding protein nucleolin in disease. RNA Biol 9: 799-808.
27. Bicknell K, Brooks G, Kaiser P, Chen H, Dove BK, et al. (2005) Nucleolin is regulated both at the level of transcription and translation. Biochem Biophys Res Commun 332: 817-822.
28. Hirano K, Miki Y, Hirai Y, Sato R, Itoh T, et al. (2005) A multifunctional shuttling protein nucleolin is a macrophage receptor for apoptotic cells. J Biol Chem 280: 39284-39293.
29. Becherel OJ, Gueven N, Birrell GW, Schreiber V, Suraweera A, et al. (2006) Nucleolar localization of aprataxin is dependent on interaction with nucleolin and on active ribosomal DNA transcription. Hum Mol Genet 15: 2239-2249.
30. Mongelard F, Bouvet P (2007) Nucleolin: a multiFACeTed protein. Trends Cell Biol 17: 80-86.
31. Durut N, Saez-Vasquez J (2015) Nucleolin: dual roles in rDNA chromatin transcription. Gene 556: 7-12.
32. Shimakami T, Honda M, Kusakawa T, Murata T, Shimotohno K, et al. (2006) Effect of hepatitis C virus (HCV) NS5B-nucleolin interaction on HCV replication with HCV subgenomic replicon. J Virol 80: 3332-3340.
33. Strang BL, Boulant S, Coen DM (2010) Nucleolin associates with the human cytomegalovirus DNA polymerase accessory subunit UL44 and is necessary for efficient viral replication. J Virol 84: 1771-1784.
34. Cancio-Lonches C, Yocupicio-Monroy M, Sandoval-Jaime C, Galvan-Mendoza I, Urena L, et al. (2011) Nucleolin interacts with the feline calicivirus 3' untranslated region and the protease-polymerase NS6 and NS7 proteins, playing a role in virus replication. J Virol 85: 8056-8068.
35. Strang BL, Boulant S, Kirchhausen T, Coen DM (2012) Host cell nucleolin is required to maintain the architecture of human cytomegalovirus replication compartments. MBio 3.
36. Bender BJ, Coen DM, Strang BL (2014) Dynamic and nucleolin-dependent localization of human cytomegalovirus UL84 to the periphery of viral replication compartments and nucleoli. J Virol 88: 11738-11747.

845 37. Chen YL, Liu CD, Cheng CP, Zhao B, Hsu HJ, et al. (2014) Nucleolin is important for
846 Epstein-Barr virus nuclear antigen 1-mediated episome binding, maintenance, and
847 transcription. Proc Natl Acad Sci U S A 111: 243-248.
848 38. Kumar D, Broor S, Rajala MS (2016) Interaction of Host Nucleolin with Influenza A Virus
849 Nucleoprotein in the Early Phase of Infection Limits the Late Viral Gene Expression.
850 PLoS One 11: e0164146.
851 39. Terrier O, Carron C, De Chassey B, Dubois J, Traversier A, et al. (2016) Nucleolin
852 interacts with influenza A nucleoprotein and contributes to viral ribonucleoprotein
853 complexes nuclear trafficking and efficient influenza viral replication. Sci Rep 6:
854 29006.
855 40. Gao Z, Hu J, Wang X, Yang Q, Liang Y, et al. (2018) The PA-interacting host protein
856 nucleolin acts as an antiviral factor during highly pathogenic H5N1 avian influenza
857 virus infection. Arch Virol.
858 41. Machin A, Martin Alonso JM, Dalton KP, Parra F (2009) Functional differences between
859 precursor and mature forms of the RNA-dependent RNA polymerase from rabbit
860 hemorrhagic disease virus. J Gen Virol 90: 2114-2118.
861 42. Urakova N, Frese M, Hall RN, Liu J, Matthaei M, et al. (2015) Expression and partial
862 characterisation of rabbit haemorrhagic disease virus non-structural proteins.
863 Virology 484: 69-79.
864 43. Leen EN, Sorgeloos F, Correia S, Chaudhry Y, Cannac F, et al. (2016) A Conserved
865 Interaction between a C-Terminal Motif in Norovirus VPg and the HEAT-1 Domain of
866 eIF4G Is Essential for Translation Initiation. PLoS Pathog 12: e1005379.
867 44. Fernandez-Vega V, Sosnovtsev SV, Belliot G, King AD, Mitra T, et al. (2004) Norwalk
868 virus N-terminal nonstructural protein is associated with disassembly of the Golgi
869 complex in transfected cells. J Virol 78: 4827-4837.
870 45. Bailey D, Kaiser WJ, Hollinshead M, Moffat K, Chaudhry Y, et al. (2010) Feline calicivirus
871 p32, p39 and p30 proteins localize to the endoplasmic reticulum to initiate replication
872 complex formation. Journal of General Virology 91: 739-749.
873 46. Hyde JL, Mackenzie JM (2010) Subcellular localization of the MNV-1 ORF1 proteins and
874 their potential roles in the formation of the MNV-1 replication complex. Virology 406:
875 138-148.
876 47. Chen J, Guo K, Kastan MB (2012) Interactions of nucleolin and ribosomal protein L26
877 (RPL26) in translational control of human p53 mRNA. J Biol Chem 287: 16467-16476.
878 48. Ahlquist P, Noueiry AO, Lee WM, Kushner DB, Dye BT (2003) Host factors in positive-
879 strand RNA virus genome replication. J Virol 77: 8181-8186.
880 49. Subba-Reddy CV, Yunus MA, Goodfellow IG, Kao CC (2012) Norovirus RNA synthesis is
881 modulated by an interaction between the viral RNA-dependent RNA polymerase and
882 the major capsid protein, VP1. J Virol 86: 10138-10149.
883 50. Thackray LB, Duan E, Lazear HM, Kambal A, Schreiber RD, et al. (2012) Critical role for
884 interferon regulatory factor 3 (IRF-3) and IRF-7 in type I interferon-mediated control
885 of murine norovirus replication. J Virol 86: 13515-13523.
886 51. Thorne LG, Goodfellow IG (2014) Norovirus gene expression and replication. J Gen Virol
887 95: 278-291.
888 52. Li TF, Hosmillo M, Schwanke H, Shu T, Wang Z, et al. (2018) Human Norovirus NS3 Has
889 RNA Helicase and Chaperoning Activities. J Virol 92.
890 53. Oliveira LM, Blawid R, Orilio AF, Andrade BYG, Souza ACA, et al. (2018) Development of
891 an infectious clone and replicon system of norovirus GII.4. J Virol Methods 258: 49-
892 53.
893 54. Urakova N, Warden AC, White PA, Strive T, Frese M (2017) A Motif in the F Homomorph
894 of Rabbit Haemorrhagic Disease Virus Polymerase Is Important for the Subcellular
895 Localisation of the Protein and Its Ability to Induce Redistribution of Golgi
896 Membranes. Viruses 9.

55. Urakova N, Strive T, Frese M (2017) RNA-Dependent RNA Polymerases of Both Virulent and Benign Rabbit Caliciviruses Induce Striking Rearrangement of Golgi Membranes. PLOS ONE 12: e0169913.
56. Fan B, Lu KY, Reymond Sutandy FX, Chen YW, Konan K, et al. (2014) A human proteome microarray identifies that the heterogeneous nuclear ribonucleoprotein K (hnRNP K) recognizes the 5' terminal sequence of the hepatitis C virus RNA. Mol Cell Proteomics 13: 84-92.
57. Nüesch JPF, Rommelaere J (2006) NS1 Interaction with CKIIα: Novel Protein Complex Mediating Parvovirus-Induced Cytotoxicity. Journal of Virology 80: 4729-4739.
58. Maggi LB, Jr., Kuchenruether M, Dadey DY, Schwope RM, Grisendi S, et al. (2008) Nucleophosmin serves as a rate-limiting nuclear export chaperone for the Mammalian ribosome. Mol Cell Biol 28: 7050-7065.
59. Robledo S, Idol RA, Crimmins DL, Ladenson JH, Mason PJ, et al. (2008) The role of human ribosomal proteins in the maturation of rRNA and ribosome production. RNA 14: 1918-1929.
60. Aminev AG, Amineva SP, Palmenberg AC (2003) Encephalomyocarditis viral protein 2A localizes to nucleoli and inhibits cap-dependent mRNA translation. Virus Res 95: 45-57.
61. Tayyari F, Marchant D, Moraes TJ, Duan W, Mastrangelo P, et al. (2011) Identification of nucleolin as a cellular receptor for human respiratory syncytial virus. Nat Med 17: 1132-1135.
62. Su PY, Wang YF, Huang SW, Lo YC, Wang YH, et al. (2015) Cell surface nucleolin facilitates enterovirus 71 binding and infection. J Virol 89: 4527-4538.
63. Balinsky CA, Schmeisser H, Ganesan S, Singh K, Pierson TC, et al. (2013) Nucleolin interacts with the dengue virus capsid protein and plays a role in formation of infectious virus particles. J Virol 87: 13094-13106.
64. Zhu J, Miao Q, Tang J, Wang X, Dong D, et al. (2018) Nucleolin mediates the internalization of rabbit hemorrhagic disease virus through clathrin-dependent endocytosis. PLoS Pathog 14: e1007383.
65. Waggoner S, Sarnow P (1998) Viral ribonucleoprotein complex formation and nucleolar-cytoplasmic relocalization of nucleolin in poliovirus-infected cells. J Virol 72: 6699-6709.
66. Sagou K, Uema M, Kawaguchi Y (2010) Nucleolin is required for efficient nuclear egress of herpes simplex virus type 1 nucleocapsids. J Virol 84: 2110-2121.
67. Shannon P, Markiel A, Ozier O, Baliga NS, Wang JT, et al. (2003) Cytoscape: a software environment for integrated models of biomolecular interaction networks. Genome Res 13: 2498-2504.

Figure legends

Figure 1. Tagging of RHDV RdRp in the viral replicon. (A) Schematic of RHDV-His/HA replicon constructs. The HA and 6×His peptide sequences are inserted into the RdRp aa sequence at 25, 82, 442, or 483 sites, respectively. **(B, D)** Effect of the inserted tag on viral

940 replicon activity. RK-13 cells were transfected with recombinant RHDV replicons.
941 Luciferase activity in cell lysates was measured at 48 hpt. Student *t*-tests and analysis of
942 variance were used for statistical analyses. *$p < 0.05$ and **$p < 0.01$. The number of cells
943 used in all replicate experiments was similar. **(C, E)** Western blotting of recombinant RHDV
944 replicons in RK-13 cells with the antibodies indicated. β-actin was used as an internal control.
945
946 **Figure 2. Affinity purification of solubilized RHDV replicase RdRp-associated host**
947 **factors. (A)** Schematic of two-step affinity purification of the RHDV replicase RdRp-
948 associated host proteins. **(B)** After two-step affinity purification, the eluted proteins were
949 resolved by SDS-PAGE. Specifically, enriched protein bands (arrows) in the RHDV-His/HA-
950 luc sample were identified by mass spectrometry. Mainly, host proteins and identified viral
951 proteins in the bands indicated are shown. Host factors selected for further study are marked
952 in red. **(C)** Network analysis of RHDV replicase-associated protein. The interaction network
953 shows the proteins identified as being associated with RHDV replicase by affinity
954 purification. To simplify these interdependencies, host factors that did not interact with other
955 factors in the network are not shown. NCL is marked in red. Proteins that interact with NCL
956 are labeled in yellow. Note: the network was generated using the data presented in Table 1.
957 The interaction network was generated using the STRING online tool and then presented
958 using Cytoscape software [67].
959
960 **Figure 3. NCL is involved in RHDV replication. (A)** The effect of NCL eukaryotic
961 plasmids on viral replicon activity. Relative luciferase activity was evaluated in RK-13 cells
962 carrying pRHDV-luc, and trans-supplemented NCL eukaryotic plasmids pFlag-NCL (0.2 μg,
963 0.4 μg) at 24 hpt and 48 hpt. The p3 × Flag-CMV-14 vector acted as negative control. The
964 luciferase activity in RK-13 cells was evaluated by measuring Fluc activity. Rluc activity was

965 measured to normalize the transfection efficiency. **(B)** The effect of NCL siRNA on viral
966 replicon activity. The RK-13 cells, co-transfected with pRHDV-luc and NCL siRNA (20
967 pmol, 40 pmol, 60 pmol, or 80 pmol), were lysed at 24 hpt and 48 hpt, and Fluc activity was
968 measured based on RLUs and normalized according to the results obtained for a co-
969 transfected pLTK plasmid encoding Rluc. The nonspecific siRNA acted as negative control.
970 **(C-D)** The effect of NCL on mRHDV replication. The RK-13 cells, transfected with pFlag-
971 NCL(1μg, 2μg) or NCL siRNA (40 pmol, 80 pmol), were infected with mRHDV (MOI = 1)
972 at 24 hpt, and the level of mRHDV replication were evaluated by WB and qRT-PCR at 48
973 hpi. The p3 × Flag-CMV-14 vector and nonspecific siRNA acted as negative control. **(E-F)**
974 The replication ability of mRHDV in RK-NCL cells. The expression level of NCL in RK-
975 NCL cells at 10 passages was determined by western blot analysis with anti-Flag mAb. The
976 RHDV replication levels in RK-NCL cells infected with mRHDV (MOI = 1) were evaluated
977 by WB and qRT-PCR at 48 hpi. RK-GFP cells acted as negative controls; RK-13 cells acted
978 as blank controls. Student *t*-tests and analysis of variance were used for statistical analyses.
979 $*p < 0.05$ and $**p < 0.01$. The number of cells used in all replicate experiments was similar.
980
981 **Figure 4. NCL interacts with RHDV RdRp. (A)** M2H interaction of NCL with RHDV
982 nonstructural proteins. Student *t*-tests and analysis of variance were used for statistical
983 analyses. $*p < 0.05$ and $**p < 0.01$. The number of cells used in all replicate experiments was
984 similar. **(B)** NCL binds to RdRp, p16 and p23 during RHDV replication. An IP assay was
985 performed on cell lysates using NCL mAb in RK-13 cells that were infected or uninfected
986 with mRHDV, then immunoblotted with Abs against NCL, RdRp, p16 or p23. β-actin was
987 used as an internal control. Cells uninfected with mRHDV served as negative controls. **(C)**
988 Validation of the interaction of RHDV RdRp with NCL in a Co-IP assay. RK-13 cells were
989 co-transfected with the indicated plasmids (+) or empty vectors (-). At 48 hpt, cells were

lysed, and IP of myc-fused proteins was performed using anti-myc mAb. Lysates (input) and IPs were analyzed with IB using antibody against myc or Flag. β-actin was used as an internal control. **(D)** Confocal microscopy analysis of NCL (green) and RdRp (red) in RK-13 cells infected with mRHDV at 24 hpi with mAbs against NCL and RdRp. The small white boxes represent amplified random co-localization spots within the merged image, and the co-localization spots are indicated with white arrowheads. **(E–F)** The functional domain of NCL interacting with RdRp was identified by GST pull-down assay. GST fusions of various NCL domains were used as bait; RdRp expressed in RK-13 cells, obtained at 48 hpt with pRdRp-myc plasmids, was used as prey. RdRp binding was immunoblotted with anti-myc mAb. The GST protein acted as a negative control. **(G–I)** IB analysis of the glutathione affinity pull-down assays was performed to map the binding domain of the RdRp protein. We used GST-tagged RdRp domains as bait and NCL expressed in RK-13 cells as prey. After extensive washing, NCL binding was determined by IB with anti-Flag mAb. The GST protein acted as a negative control. The interactions are shown in red. (**J**) Modeling of the functional area of NCL-RdRp interaction.

Figure 5. NCL interacts with RHDV p16. (A) We identified the interaction between RHDV p16 and NCL using Co-IP assay. RK-13 cells were co-transfected with the indicated plasmids (+) or empty vectors (-). Cell lysates were prepared 48 h post-transfection and the proteins were subjected to IP followed by IB analysis. **(B)** Confocal microscopy analysis of NCL (green) and RdRp (red) in RK-13 cells infected with mRHDV at 24 hpi with Abs against NCL and p16. The small white boxes represent amplified random co-localization spots within the merged image, and the co-localization spots are indicated with white arrowheads. **(C–D)** The functional domain of NCL interacting with p16 was identified by GST pull-down assays. GST fusions of various NCL domains were used as bait, and myc fusion-p16 proteins

expressed in RK-13 cells, were used as prey. p16 binding was immunoblotted with anti-myc mAb. The GST protein acted as a negative control. **(E–G)** Glutathione affinity pull-down assays were performed to map the binding domain of p16 protein. We used GST-tagged p16 domains as bait and Flag fusion-NCL proteins expressed in RK-13 cells as prey. After extensive washing, NCL binding was determined by IB with anti-Flag mAb. The GST protein acted as a negative control. The interactions are shown in red.

Figure 6. NCL interacts with RHDV p23. (A) Co-IP of RHDV p23 with NCL in RK-13 cells. RK-13 cells were transfected with the indicated plasmids (+) (myc-p23 or Flag-NCL) and empty vectors (-) for 48 h. Cell lysates were incubated with anti-myc mAb-coated beads and Co-IP proteins were subjected to IB analysis. **(B)** Confocal microscopy analysis of NCL (green) and p23 (red) in RK-13 cells infected with mRHDV at 24 hpi with Abs against NCL and p23. The small white box represents amplified random co-localization spots within the merged image, and the co-localization spot is indicated with a white arrowhead. **(C–D)** The functional domain of NCL interacting with p23 was identified using GST pull-down assays. GST fusions of various NCL domains were used as bait, and myc fusion-p23 proteins expressed in RK-13 cells were used as prey. p23 binding was immunoblotted with anti-myc mAb. The GST protein acted as a negative control. **(E–F)** Glutathione affinity pull-down assays were performed to map the binding domain of p23 protein. We used GST-tagged p23 domains as bait and Flag fusion-NCL proteins expressed in RK-13 cells as prey. After extensive washing, NCL binding was determined by IB with anti-Flag mAb. The GST protein acted as a negative control. The interactions are shown in red. (**G**) Modeling of the functional area of NCL-p23 interaction.

Figure 7. Interactions between NCL and RdRp, p16, and p23 are required for RHDV replication. (A) The RHDV replicon and its mutants were transfected with RK-13 cells for 24 h and then lysed to detect luciferase activity in the lysate. Rluc activity was measured to normalize the transfection efficiency. **(B)** Relative luciferase activity in RK-NCL-NTD cells, RK-NCL-RBD cells, and RK-NCL-CTD cells carrying pRHDV-luc at 12, 24, 36, 48, 60, and 72 h post-transfection. RK-NCL cells acted as positive controls; RK-GFP cells acted as negative controls; RK-13 cells acted as blank controls. **(C)** RHDV mRNA levels in RK-NCL cells infected with mRHDV (MOI = 0.1) were evaluated by qRT-PCR at 12, 24, 36, 48, 60, and 72 hpi. RK-GFP cells acted as negative controls; RK-13 cells acted as blank controls. **(D)** Relative luciferase activity was evaluated in RK-13 cells carrying pRHDV-luc, treated with p16 peptide, RdRp peptide, non-specific peptide, or PBS, at 24 hpt. The non-specific peptide and PBS acted as negative controls. **(E)** The effect of RK-13 cell treated with p16 peptide, RdRp peptide, non-specific peptide or PBS on RHDV replication. The mRNA levels in RK-13 cells infected with mRHDV (MOI = 0.1) were evaluated by qRT-PCR at 24 hpi. Student *t*-tests and analysis of variance were used for statistical analyses. $*p < 0.05$ and $**p < 0.01$. The number of cells used in all replicate experiments was similar. **(F)** Schematic diagram of animal experiments. **(G)** Survival of rabbits infected with RHDV JX/CHA/97. All rabbits were challenged intramuscularly with 100 LD50 of RHDV. At 2 hpi, rabbits were injected with RdRp peptide (1 mg), p16 peptide (1 mg), non-specific peptide (1 mg), or PBS, via the ear vein, and subsequently clinically examined daily for 7 days.

Figure 8. Identification of interactions between RHDV nonstructural proteins and host factors of RCs. (A) Identification of these interactions by M2H assays. Bait and prey plasmids were co-transfected with pG5luc plasmids into subconfluent 293T cells at a molar ratio of 1:1:1 for the pACT: pBIND: pG5luc vector. At 48 h after transfection, the 293T cells

were lysed, and Rluc and Fluc activities were evaluated using the Promega Dual-Luciferase Reporter Assay System. Student *t*-tests and analysis of variance were used for statistical analyses. *$p < 0.05$ and **$p < 0.01$. The number of cells used in all replicate experiments was similar. **(B)** These interactions were verified using Co-IP assays. RK-13 cells were co-transfected with bait and prey plasmids. Cell lysates were prepared 48 h post-transfection and the proteins were subjected to IP followed by IB analysis. myc fusion proteins acted as bait proteins and Flag fusion proteins acted as prey proteins. **(C)** Effect of RdRp peptide and NCL siRNA on p23 and p16 in the RHDV RC. A series of HA tag affinity purification analyses were performed by transfection with the RHDV-luc-His/HA replicon in RK-13 cells, which were treated with RdRp peptide, NCL siRNA or PBS respectively, and in RK-NCL cells. Subsequently, the eluate proteins were subjected to IB analysis using RdRp, p16, p23 or NCL antibodies. PBS acted as a negative control; β-actin acted as an internal control. **(D)** RdRp peptide and NCL siRNA inhibited the formation of the RHDV RC. After HA tag affinity purification, the eluted proteins were resolved by SDS-PAGE. The protein bands were visualized with silver staining. PBS acted as a negative control; β-actin acted as an internal control and was detected by IB with mAb against β-actin.

Figure 9. Schematic of the role of NCL in RHDV replication. (1) RHDV is internalized into the cell. (2) Uncoating of the viral genome. (3) Translation of the polyprotein precursor. (4) Polyproteins are cleaved into nonstructural and structural proteins. (5) RHDV genomic RNA is replicated in the RC. (6) Assembly of the structural proteins and genomic RNA. Components within the dashed line are the main components of the RHDV RC. The two-way arrow represents interaction between the two proteins.

1087

1088 ## Supporting information

1089 **S1 Fig. RHDV RdRp protein structure analysis.** For clarity, the structure of the RHDV
1090 RdRp was obtained from the Protein Data Bank under the identification number 1khv
1091 (https://www.rcsb.org/). The structure of the RdRp mutation, as predicted by the SWISS-
1092 MODEL online tool (https://www.swissmodel.expasy.org/) and based on homology
1093 molecules found in the Protein Data Bank. The orange portion indicated by the red arrow is
1094 the inserted label.

1095 **S2 Fig. Effect of NCL siRNA on RK-13 cells. (A)** After RK-13 cells were transfected with
1096 different amounts of NCL siRNA for 24 h, the number and activity of viable cells were
1097 detected using CCK-8. **(B)** In different doses of NCL siRNA-treated RK-13 cells, we
1098 transfected the RHDV replicon reference plasmid pRluc. After 24 hpt, cell lysates were
1099 collected and the activity of Rluc was detected using a dual luciferase reporter system.
1100 Student t-tests and analysis of variance were used for statistical analyses. *$p < 0.05$ and **$p <$
1101 0.01. The number of cells used in all replicate experiments was similar.

1102 **S3 Fig. Alignments of amino acid sequences of G1.1a–G1.2 genogroups of RHDV. (A)**
1103 Alignments of amino acid sequences 448–478 of RdRp protein of G1.1a–G1.2 genogroups of
1104 RHDV. The representative strains used in the alignments are G1.1a: RHDV strain

JX/CHA/97 (GenBank accession no. DQ205345.1) and RHDV isolate K5_08Q712_BatchRelease1/2008 (GenBank accession no. MF598301); G1.1b: RHDV strain CB194_Pt (GenBank accession no. JX886001) and RHDV-SD (GenBank accession no. Z29514.1); G1.1c: RHDV isolate BlueGums-2 (GenBank accession no. KT280058) and RHDV isolate AUS/NSW/OUR-1/2014/06 (GenBank accession no. KY628318); G1.1d: RHDV-FRG (GenBank accession no. M67473) and RHDV-FRG/2000 (GenBank accession no. NC001543); G1.2: RHDV isolate CBAlgarve14-1 (GenBank accession no. KM115714) and RHDV isolate BLMT-1 (GenBank accession no. KT280060). Sequence alignment was performed with the ClustalW algorithm (http://www.clustal.org/). The conserved NCL-binding motif is boxed. Selected amino acids from this motif are indicated with RHDV RdRp numbering. **(B)** Alignments of representative amino acid sequences of the p16 protein of G1.1a–G1.2 genogroups of RHDV. Sequence alignment was performed with the ClustalW algorithm. The conserved NCL-binding motif is boxed. Selected amino acids from this motif are indicated with RHDV p16 numbering. **(C)** Alignments of representative amino acid sequences of p23 protein of G1.1a–G1.2 genogroups of RHDV. Sequence alignment was performed with the ClustalW algorithm. The conserved NCL-binding motif is boxed. Selected amino acids from this motif are indicated with RHDV p23 numbering.

S4 Fig. Expression level of the domain of NCL in overexpression cells. (A) The positive rate of cells was observed under a fluorescence microscope. GFP-fused NCL domain (NTD,

1124 RBD, or CTD) was expressed in RK13-NCL-NTD, RK13-NCL-RBD, and RK13-NCL-CTD

1125 cells, respectively. **(B)** The expression level of the domains of NCL in the overexpression

1126 cells at 10 passages were determined by western blot analysis with anti-Flag mAb. RK13-

1127 GFP cells were used as positive control. β-actin was used as an internal control.

1128 **S1 Table. Plasmid construct details.**

1129 (XLSX)

1130 **S2 Table. Oligonucleotide primer sequences.**

1131 (XLSX)

1132 **S3 Table. Details of protein expression.**

1133 (XLSX)

1134

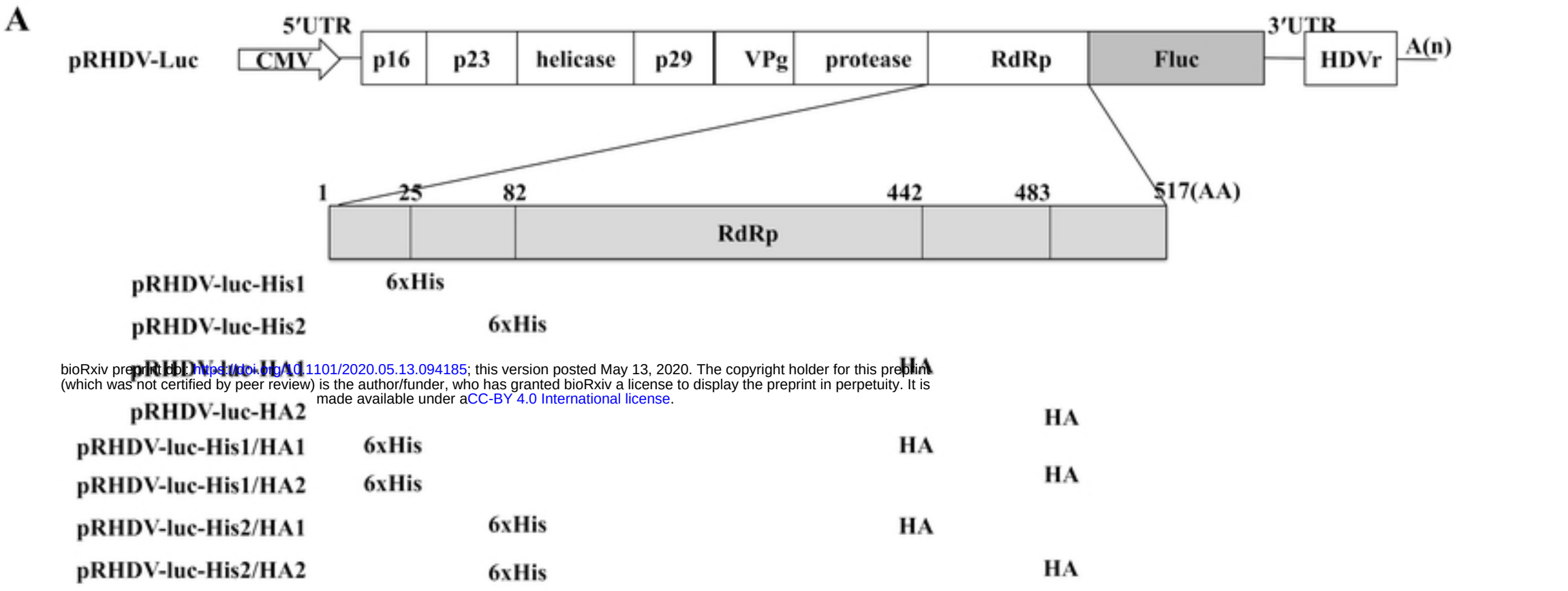

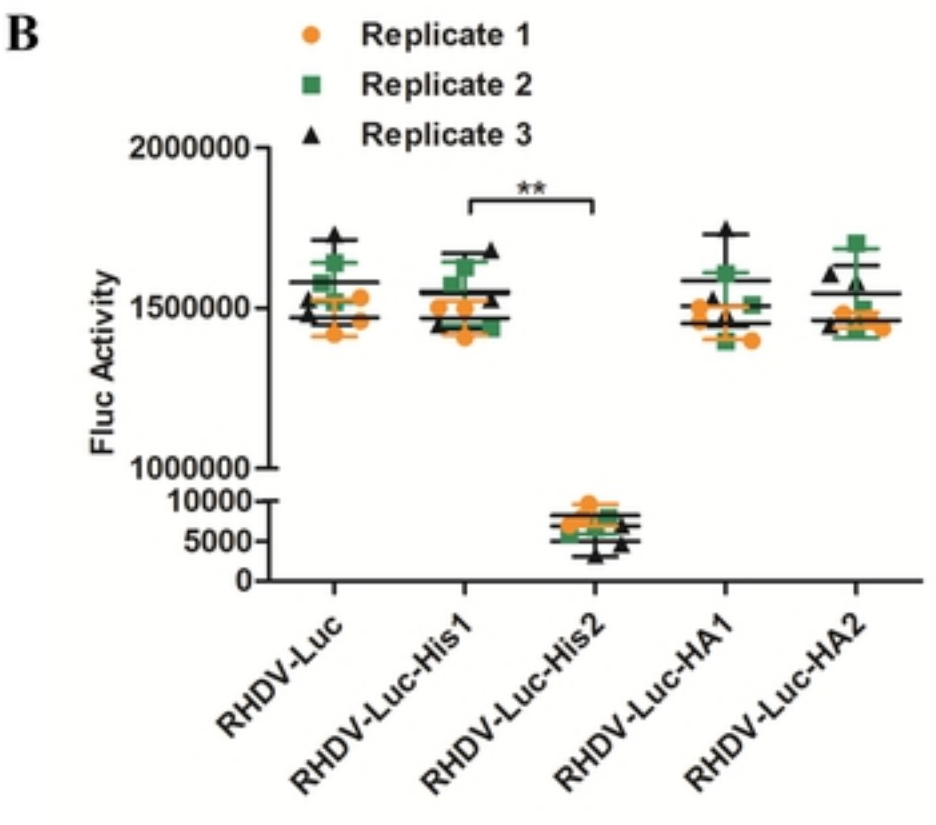

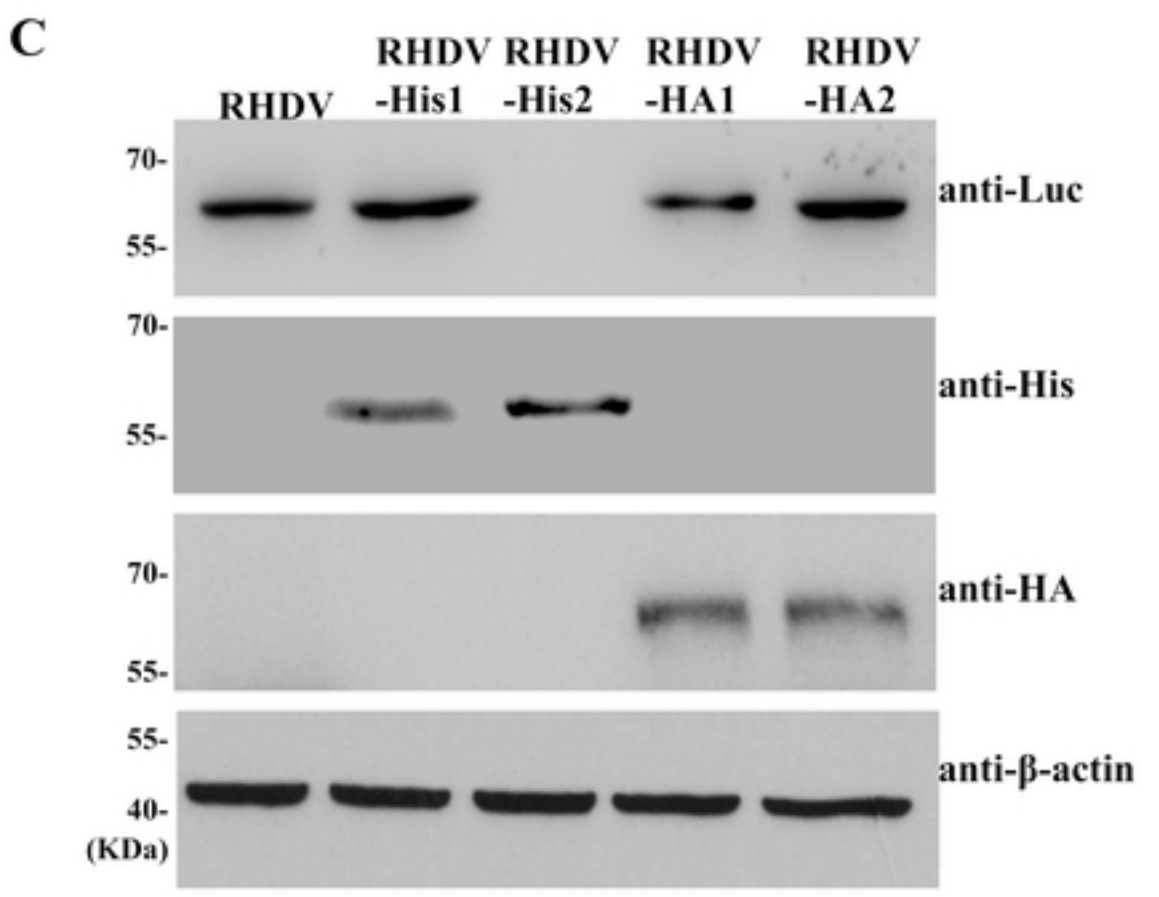

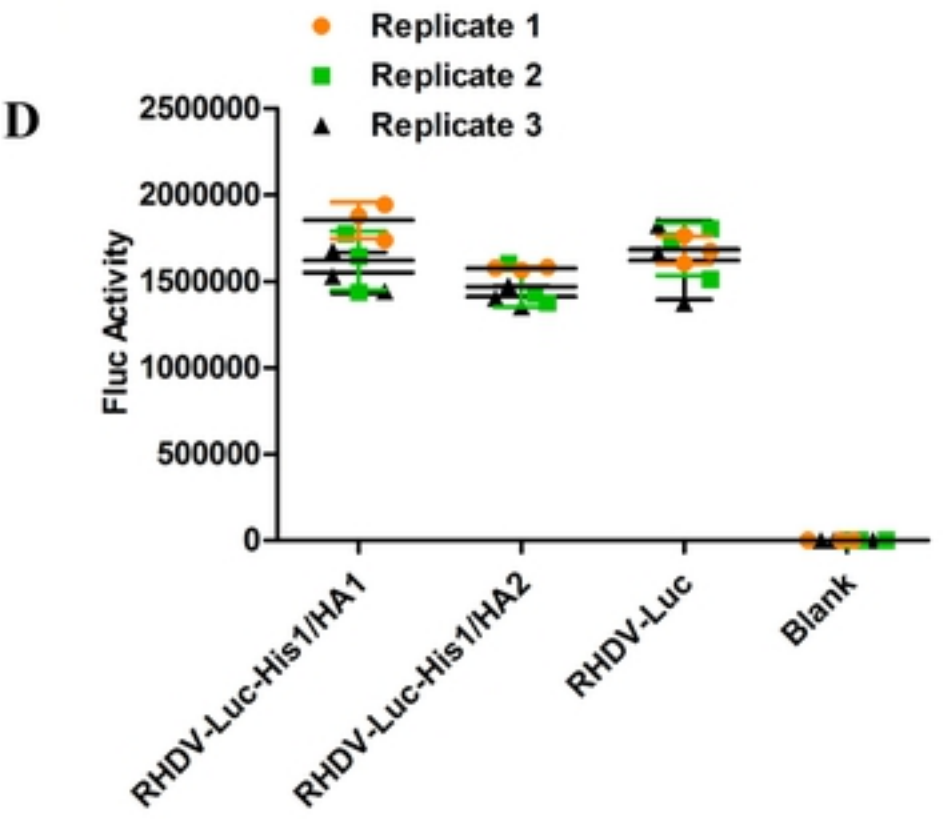

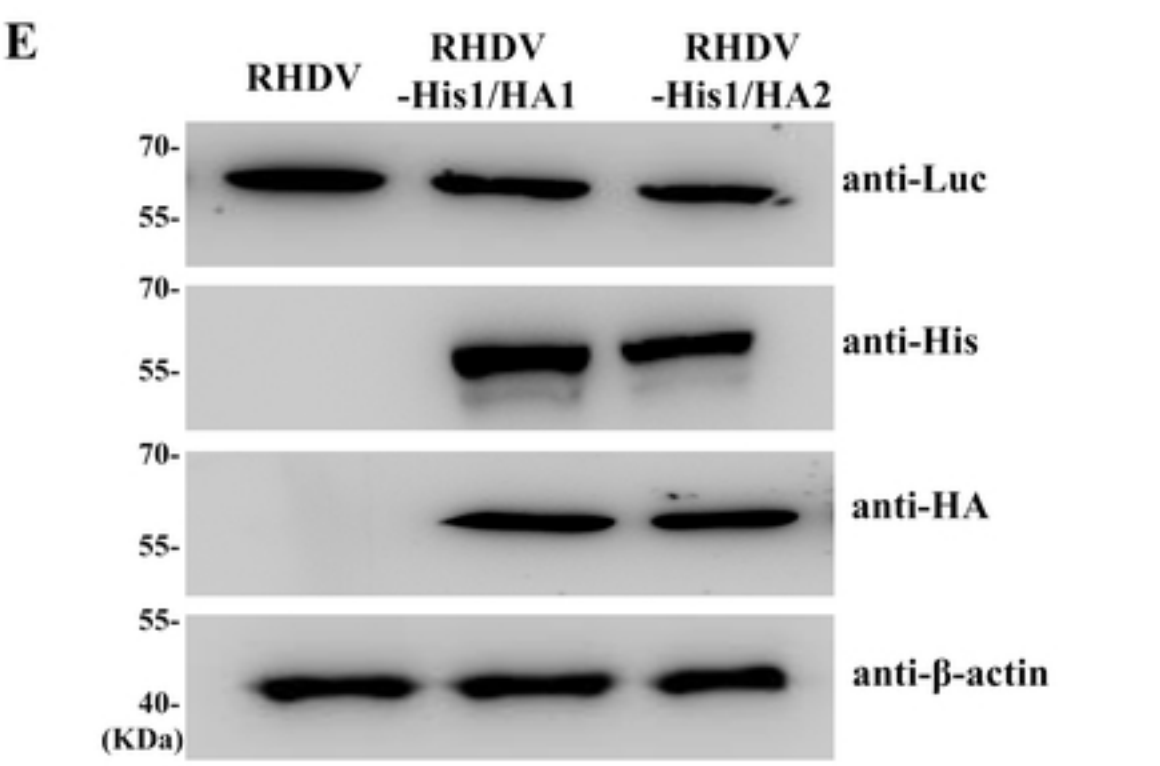

Fig 1

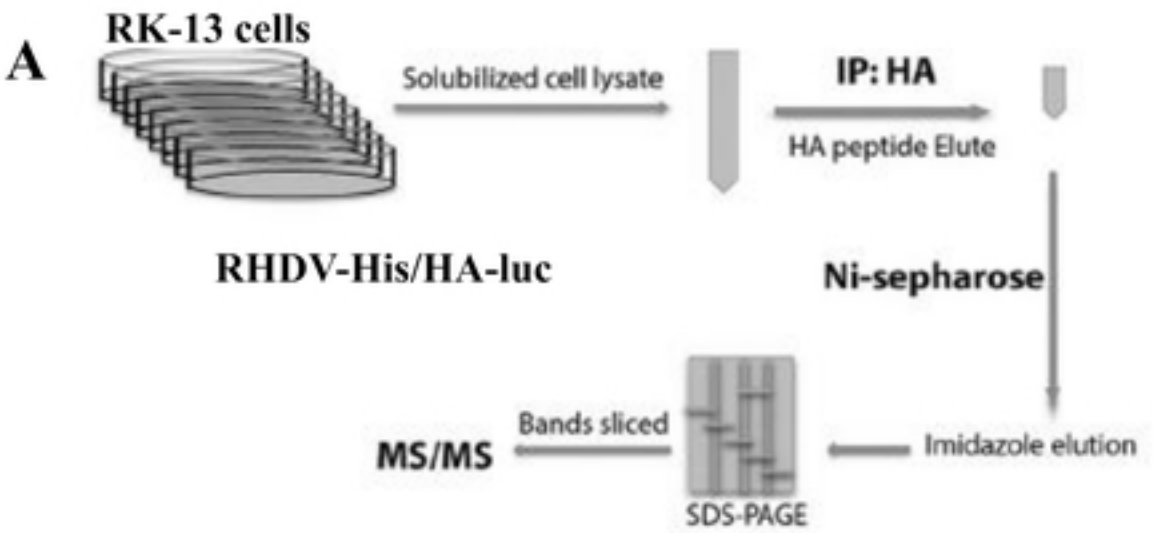
A
RK-13 cells
Solubilized cell lysate
IP: HA
HA peptide Elute
RHDV-His/HA-luc
Ni-sepharose
MS/MS
Bands sliced
Imidazole elution
SDS-PAGE

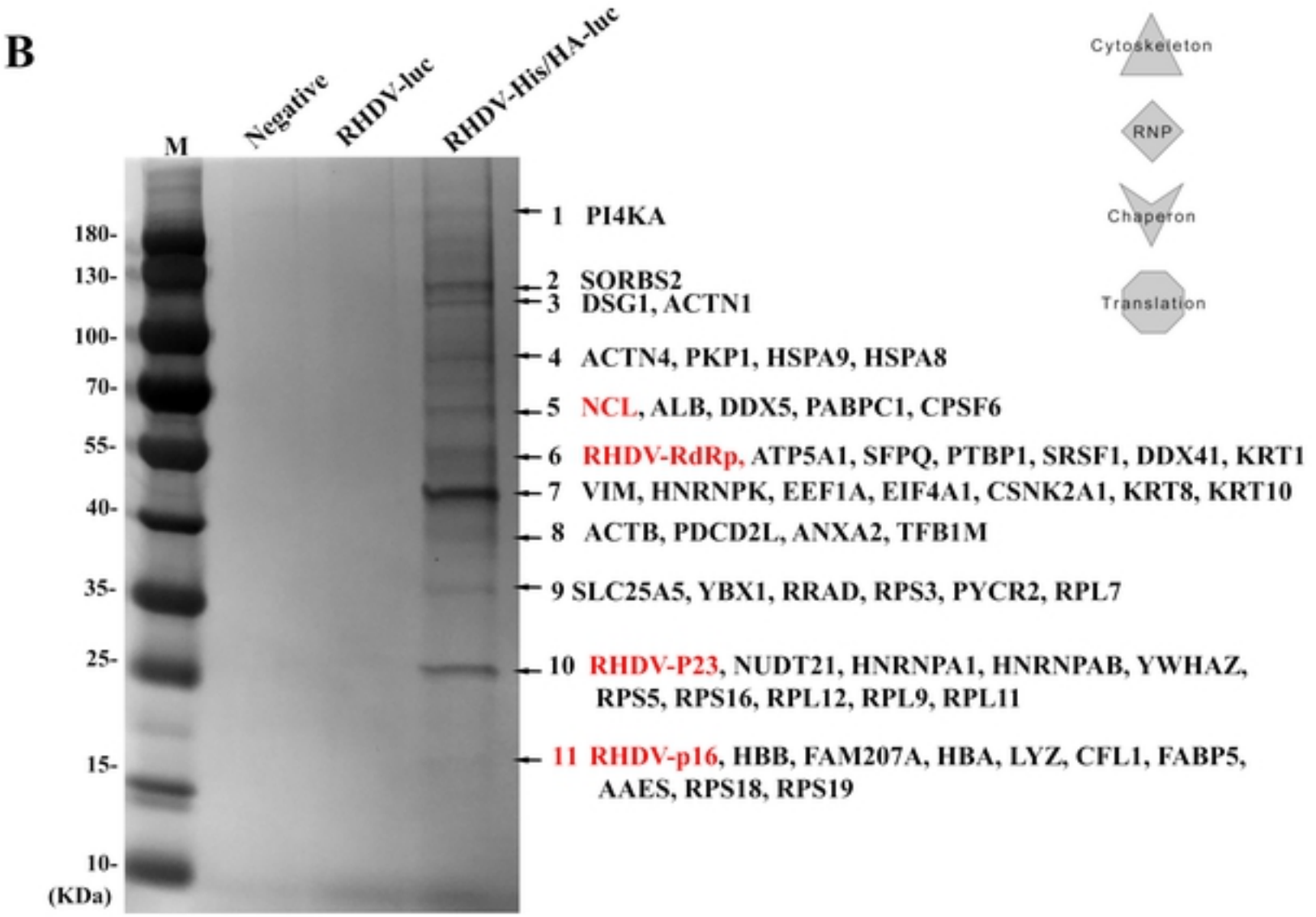
B
M
Negative
RHDV-luc
RHDV-His/HA-luc
180-
130-
100-
70-
55-
40-
35-
25-
15-
10-
(KDa)
1 PI4KA
2 SORBS2
3 DSG1, ACTN1
4 ACTN4, PKP1, HSPA9, HSPA8
5 NCL, ALB, DDX5, PABPC1, CPSF6
6 RHDV-RdRp, ATP5A1, SFPQ, PTBP1, SRSF1, DDX41, KRT1
7 VIM, HNRNPK, EEF1A, EIF4A1, CSNK2A1, KRT8, KRT10
8 ACTB, PDCD2L, ANXA2, TFB1M
9 SLC25A5, YBX1, RRAD, RPS3, PYCR2, RPL7
10 RHDV-P23, NUDT21, HNRNPA1, HNRNPAB, YWHAZ, RPS5, RPS16, RPL12, RPL9, RPL11
11 RHDV-p16, HBB, FAM207A, HBA, LYZ, CFL1, FABP5, AAES, RPS18, RPS19

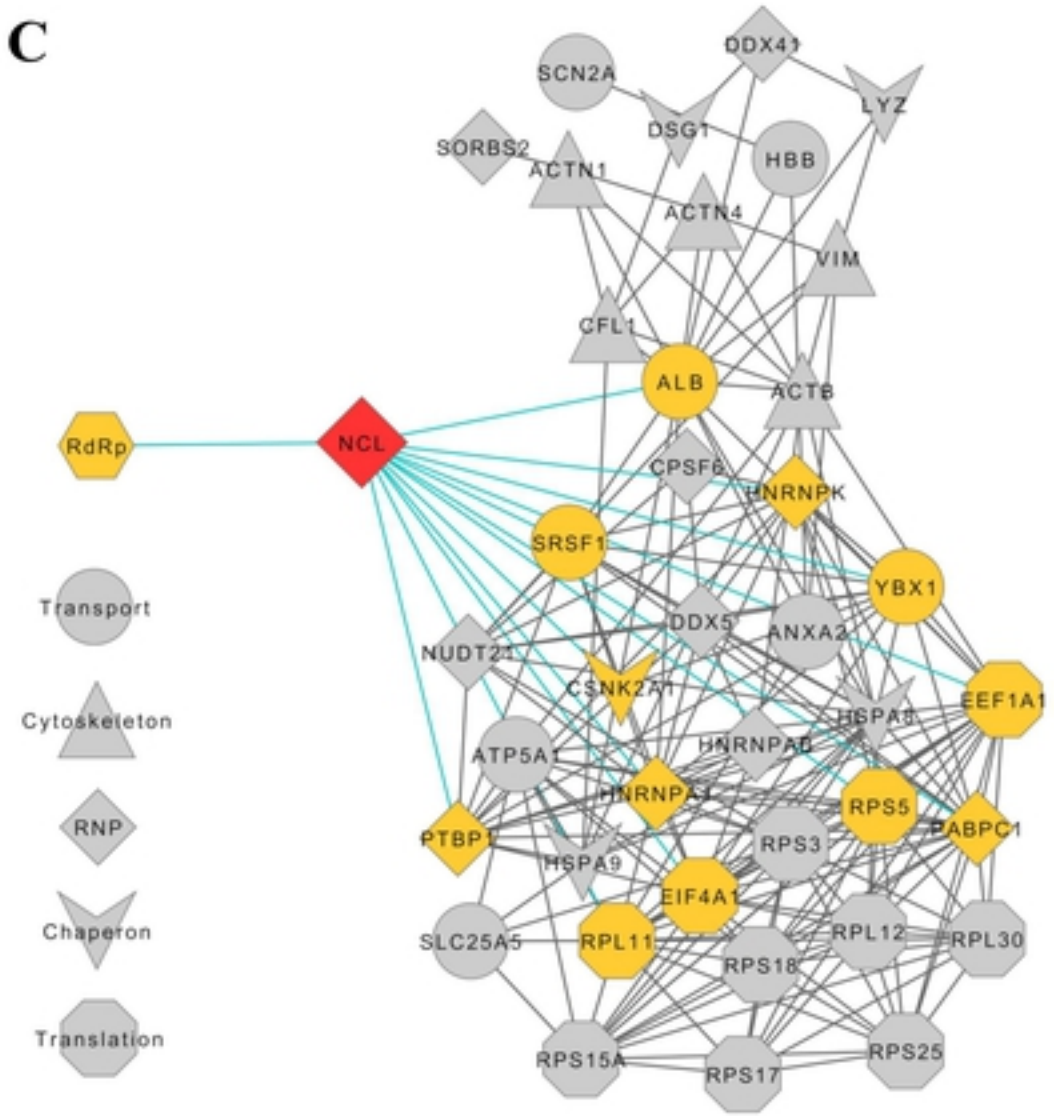
C
RdRp
Transport
Cytoskeleton
RNP
Chaperon
Translation
NCL
DDX41
SCN2A
LYZ
DSG1
SORBS2
HBB
ACTN1
ACTN4
VIM
CFL1
ALB
ACTB
CPSF6
HNRNPK
SRSF1
YBX1
DDX5
ANXA2
NUDT21
CSNK2A1
EEF1A1
HSPA8
ATP5A1
HNRNPAB
HNRNPA1
RPS5
PABPC1
PTBP1
RPS3
HSPA9
EIF4A1
SLC25A5
RPL11
RPL12
RPL30
RPS18
RPS15A
RPS17
RPS25

Fig 2

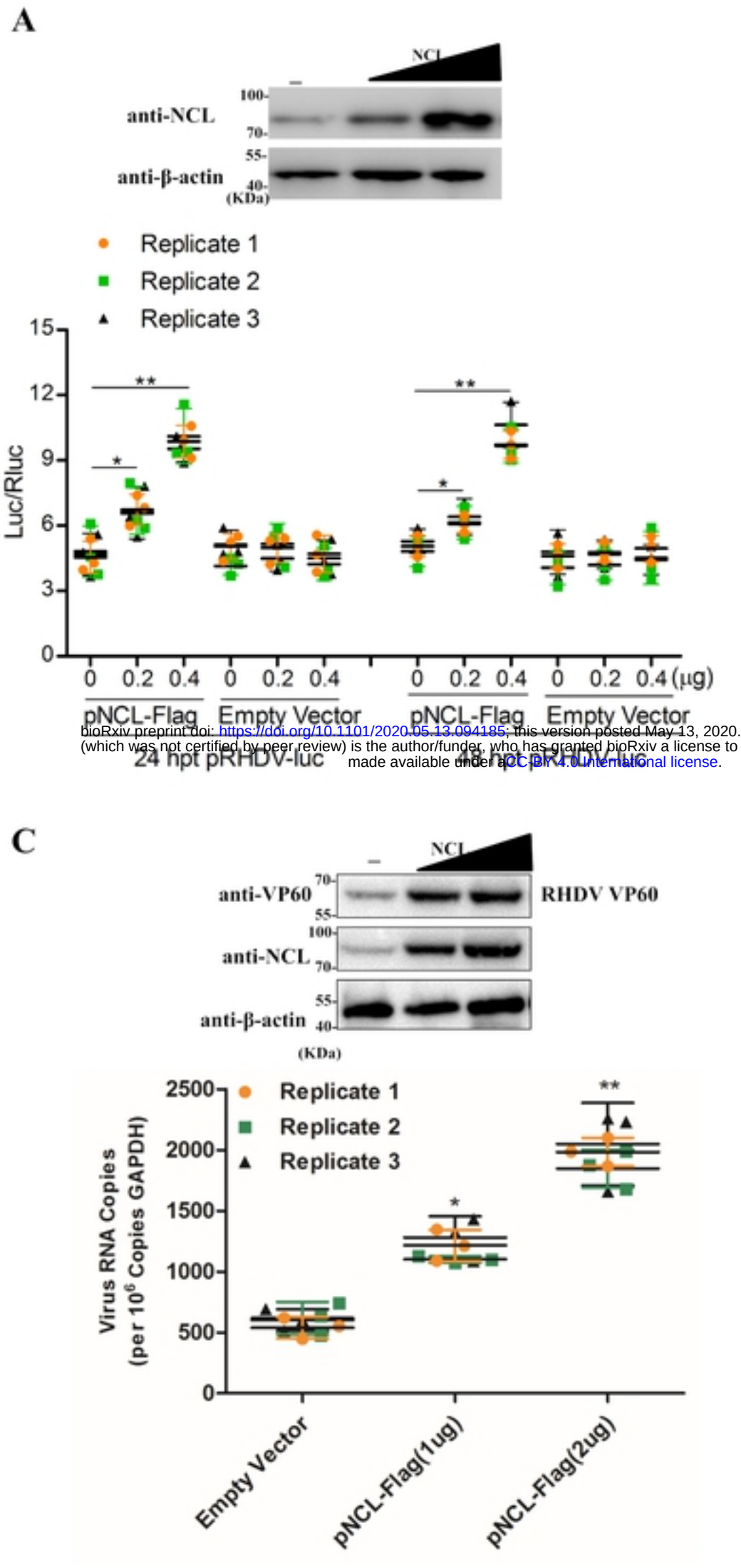

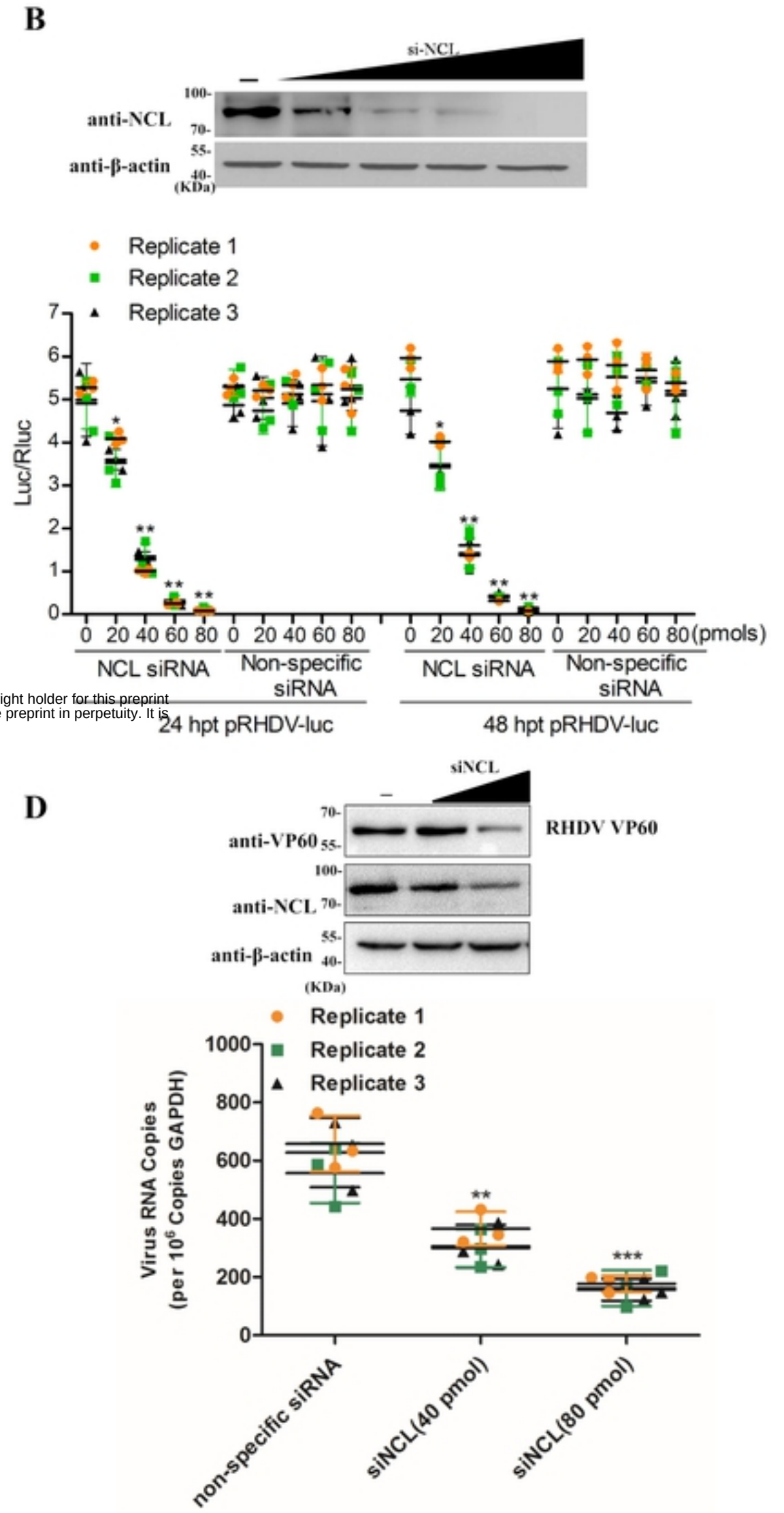

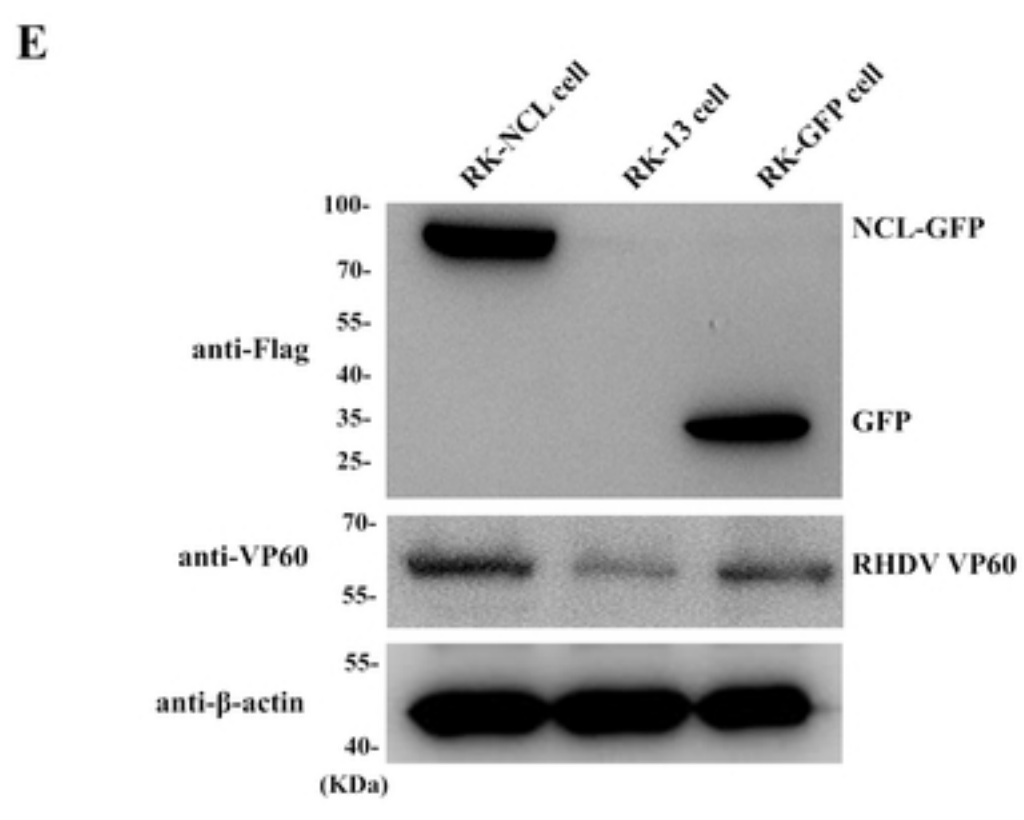

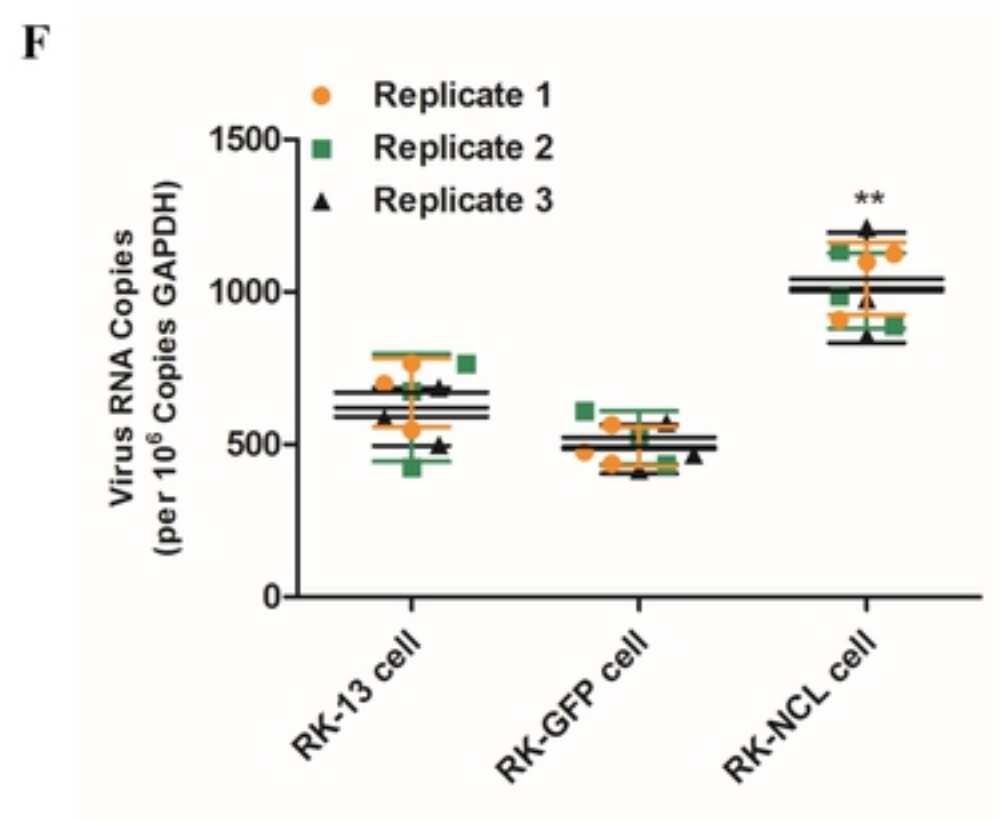

Fig 3

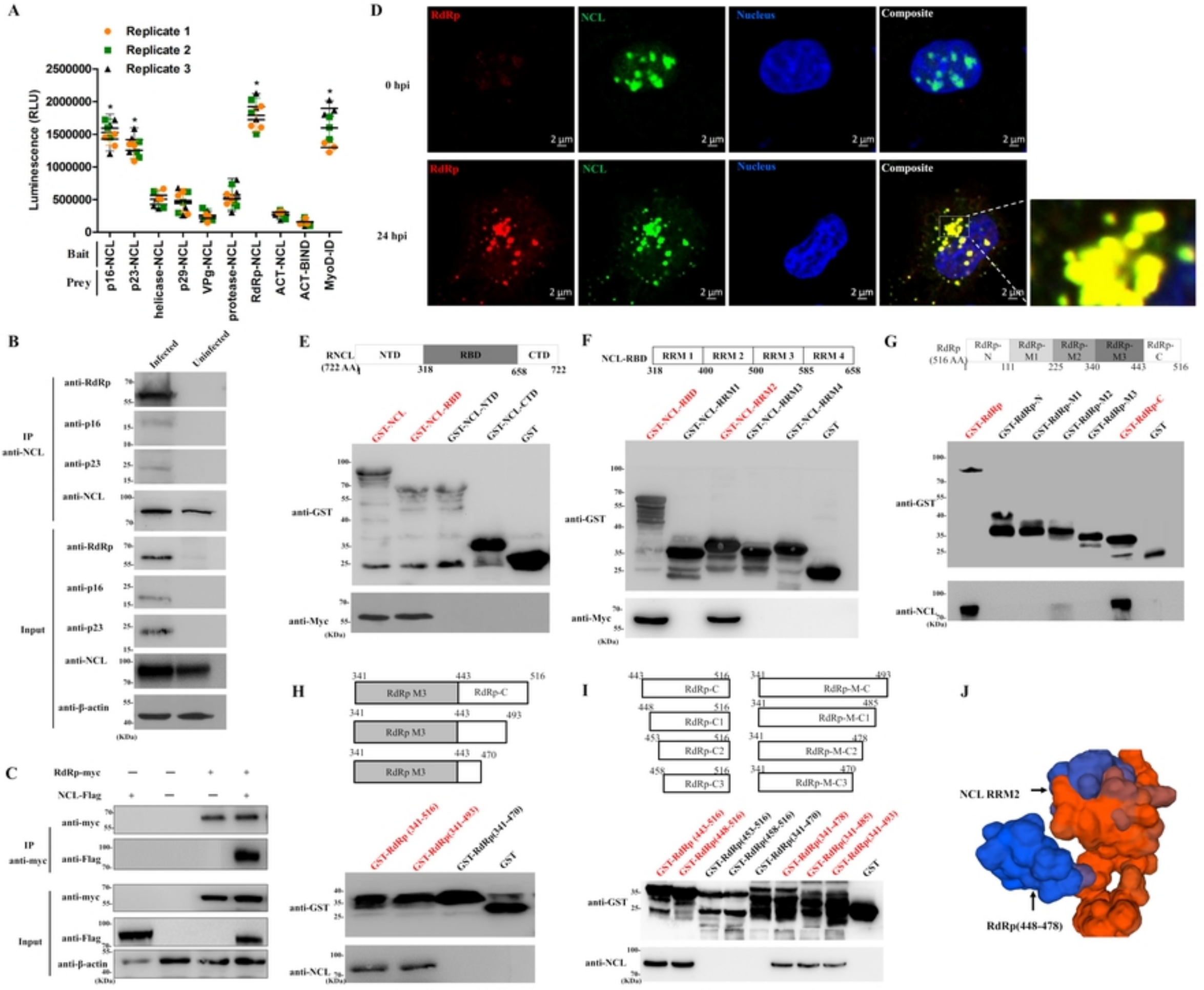
A
Replicate 1
Replicate 2
Replicate 3
Luminescence (RLU)
2500000
2000000
1500000
1000000
500000
0
Bait
Prey
p16-NCL
p23-NCL
helicase-NCL
p29-NCL
VPg-NCL
protease-NCL
RdRp-NCL
ACT-NCL
ACT-BIND
MyoD-ID
D
0 hpi
24 hpi
RdRp
NCL
Nucleus
Composite
2 μm
B
Infected
Uninfected
IP
anti-NCL
anti-RdRp
anti-p16
anti-p23
anti-NCL
Input
anti-RdRp
anti-p16
anti-p23
anti-NCL
anti-β-actin
(KDa)
E
RNCL
(722 AA)
NTD
RBD
CTD
318
658
722
GST-NCL
GST-NCL-RBD
GST-NCL-NTD
GST-NCL-CTD
GST
anti-GST
anti-Myc
(KDa)
F
NCL-RBD
RRM 1
RRM 2
RRM 3
RRM 4
318
400
500
585
658
GST-NCL-RBD
GST-NCL-RRM1
GST-NCL-RRM2
GST-NCL-RRM3
GST-NCL-RRM4
GST
anti-GST
anti-Myc
(KDa)
G
RdRp
(516 AA)
RdRp-N
RdRp-M1
RdRp-M2
RdRp-M3
RdRp-C
1
111
225
340
443
516
GST-RdRp
GST-RdRp-N
GST-RdRp-M1
GST-RdRp-M2
GST-RdRp-M3
GST-RdRp-C
GST
anti-GST
anti-NCL
(KDa)
C
RdRp-myc
NCL-Flag
IP
anti-myc
anti-myc
anti-Flag
Input
anti-myc
anti-Flag
anti-β-actin
(KDa)
H
RdRp M3
RdRp-C
341
443
493
470
516
GST-RdRp (341-516)
GST-RdRp(341-493)
GST-RdRp(341-470)
GST
anti-GST
anti-NCL
(KDa)
I
RdRp-C
RdRp-C1
RdRp-C2
RdRp-C3
RdRp-M-C
RdRp-M-C1
RdRp-M-C2
RdRp-M-C3
443
448
453
458
516
341
485
478
470
493
GST-RdRp (443-516)
GST-RdRp(448-516)
GST-RdRp(453-516)
GST-RdRp(458-516)
GST-RdRp(341-478)
GST-RdRp(341-485)
GST-RdRp(341-493)
GST
anti-GST
anti-NCL
(KDa)
J
NCL RRM2
RdRp(448-478)

Fig 4

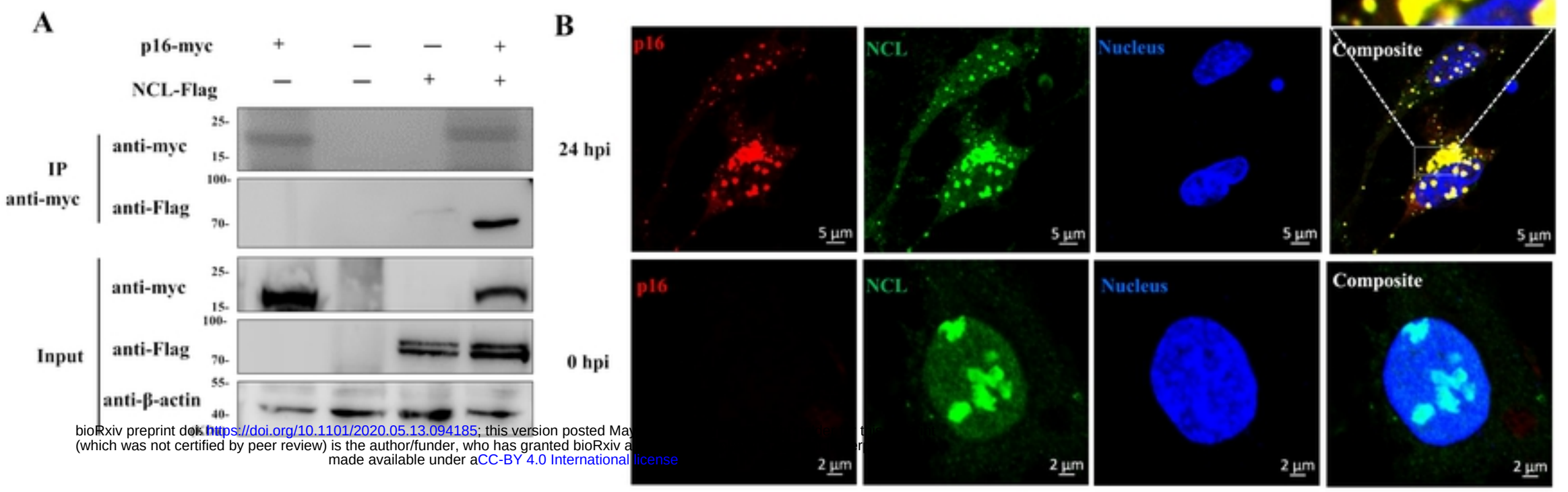

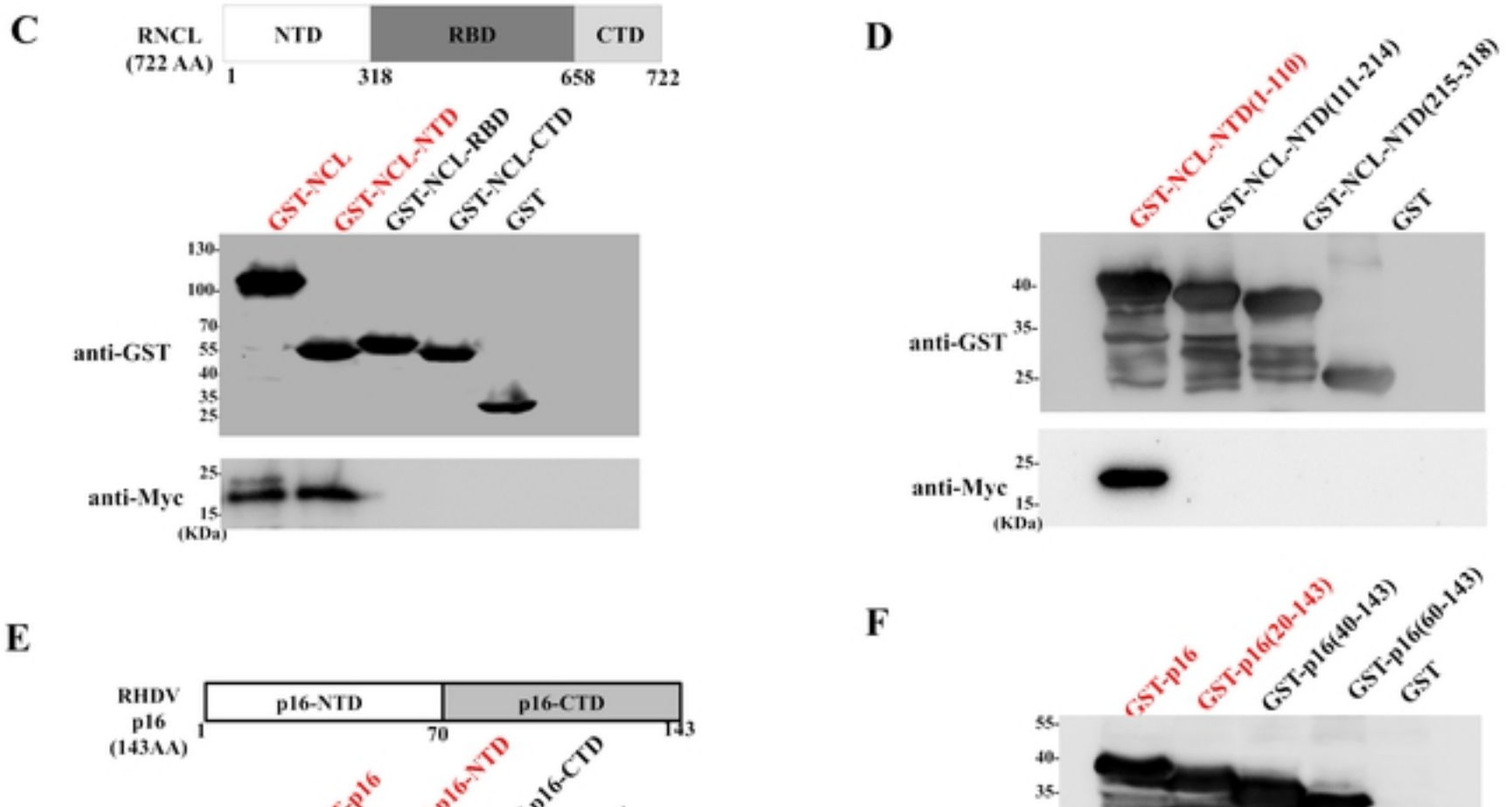

Fig 5

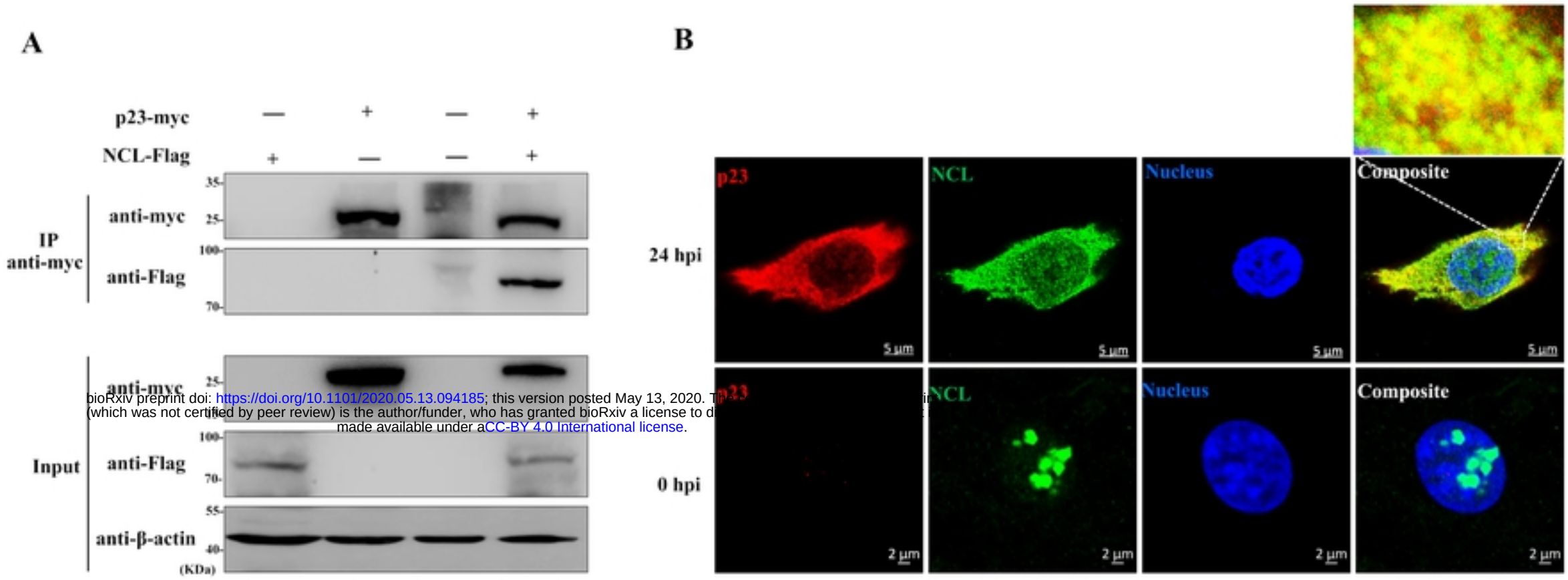

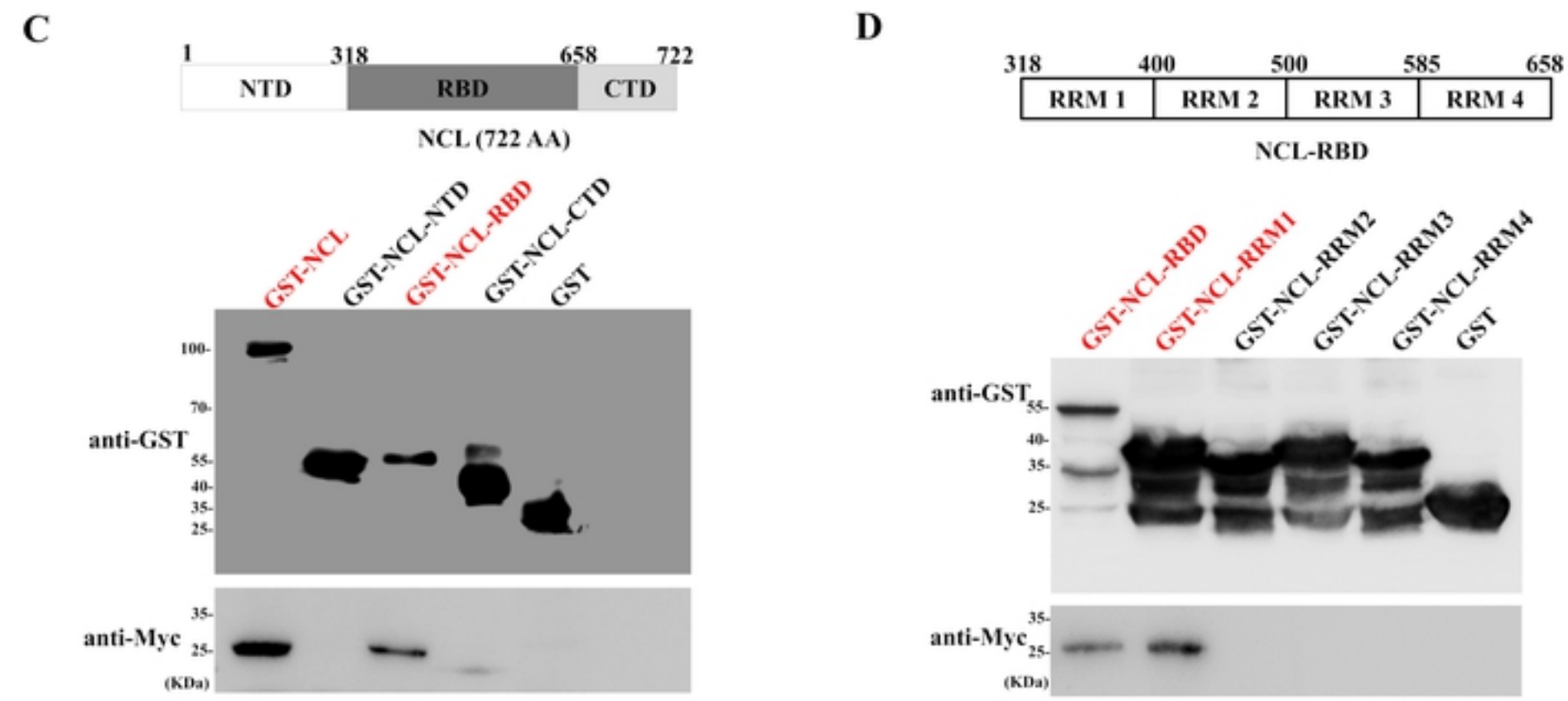

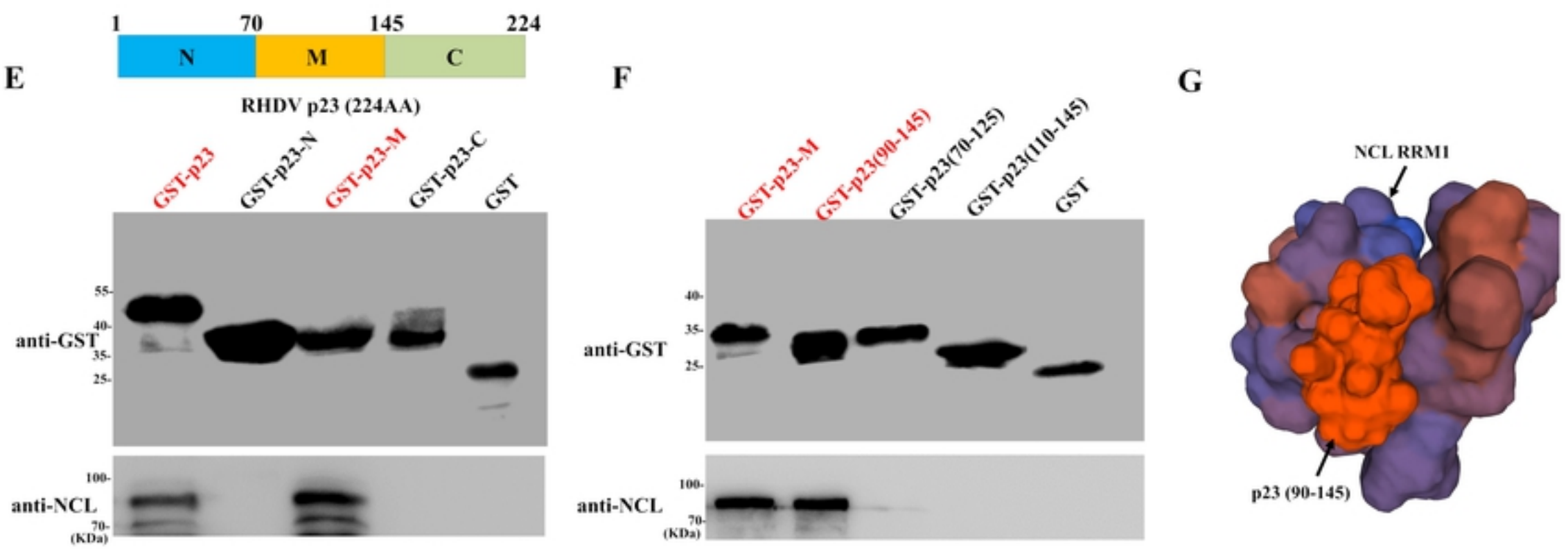

Fig 6

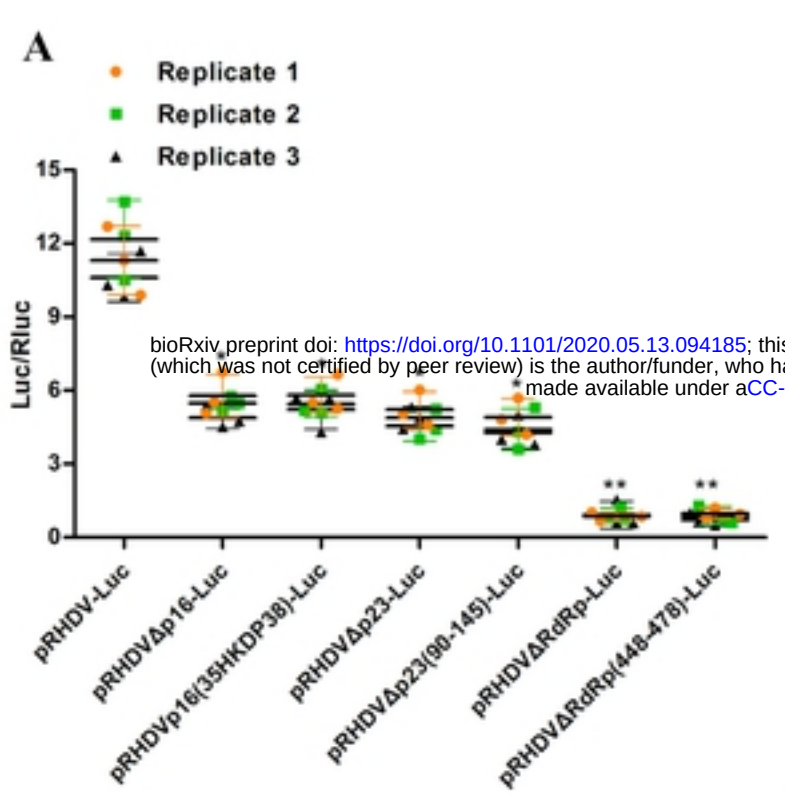

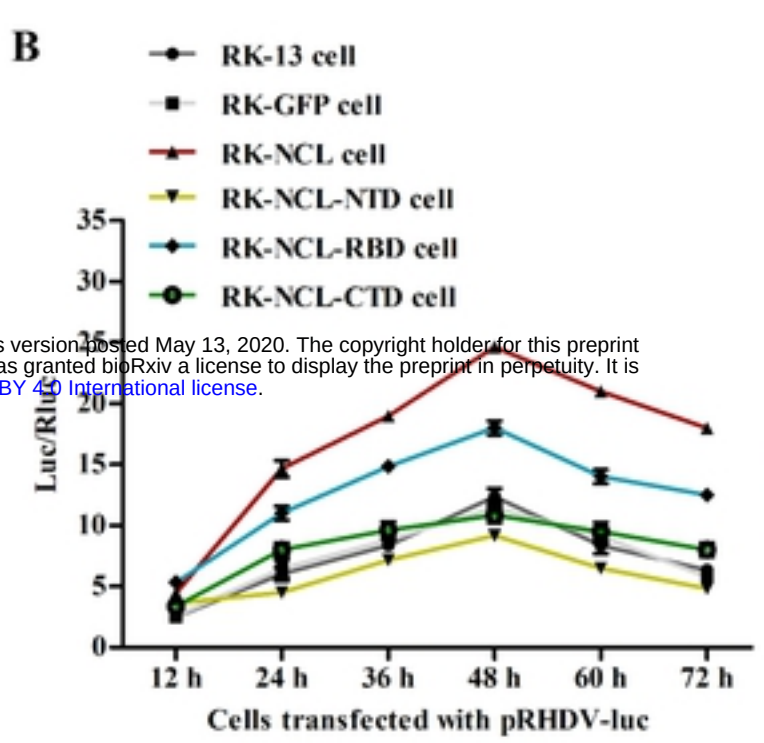

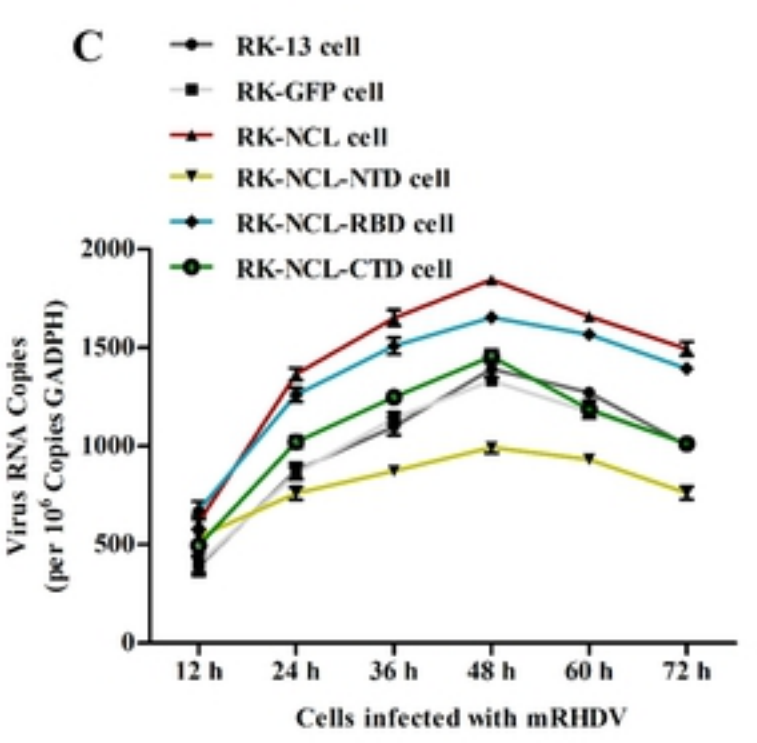

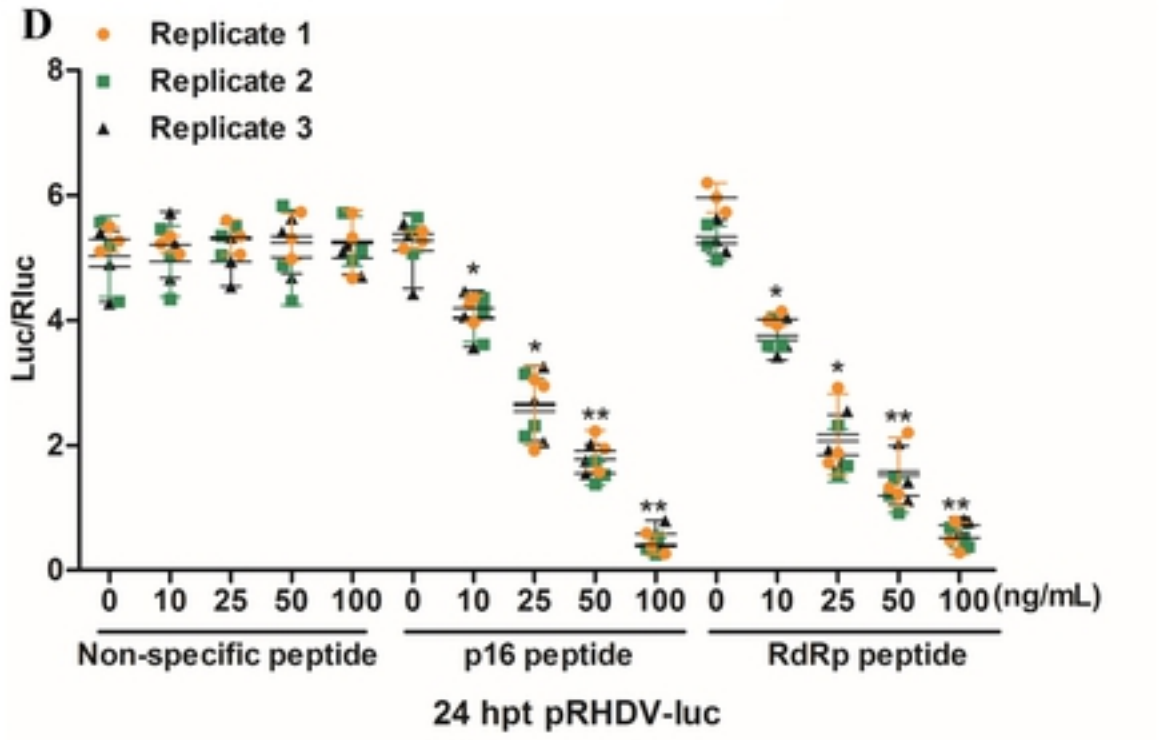

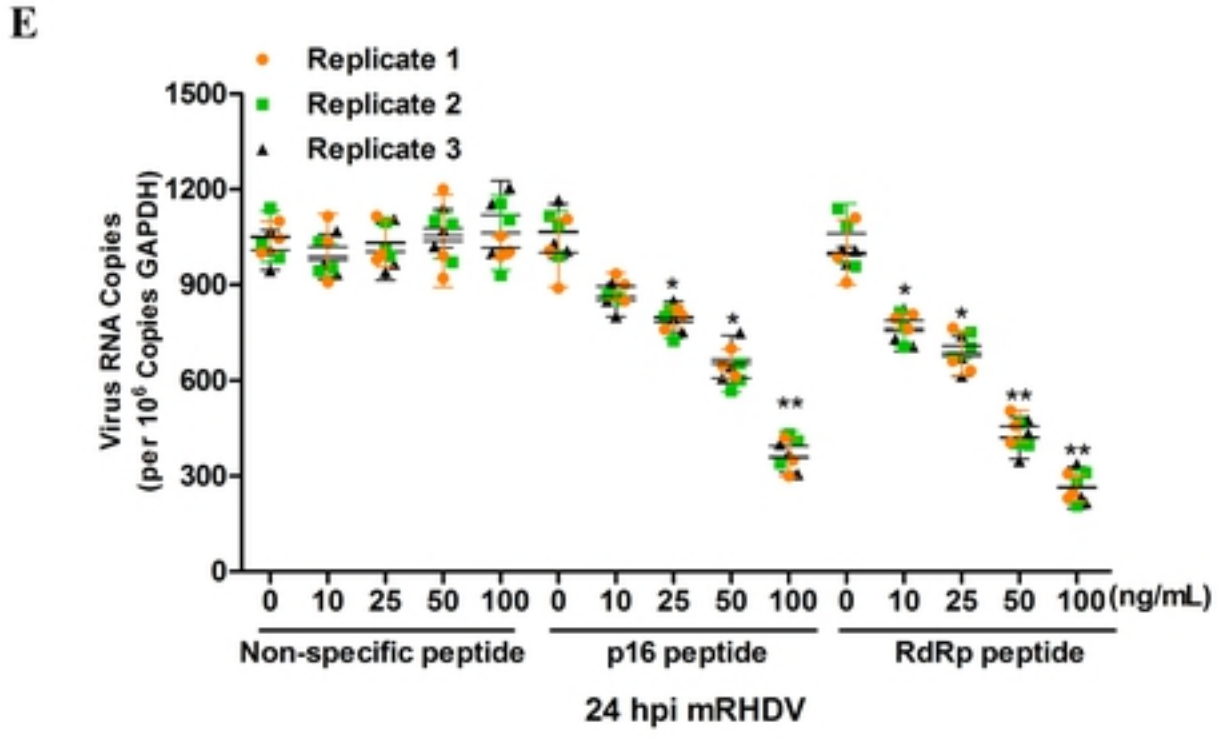

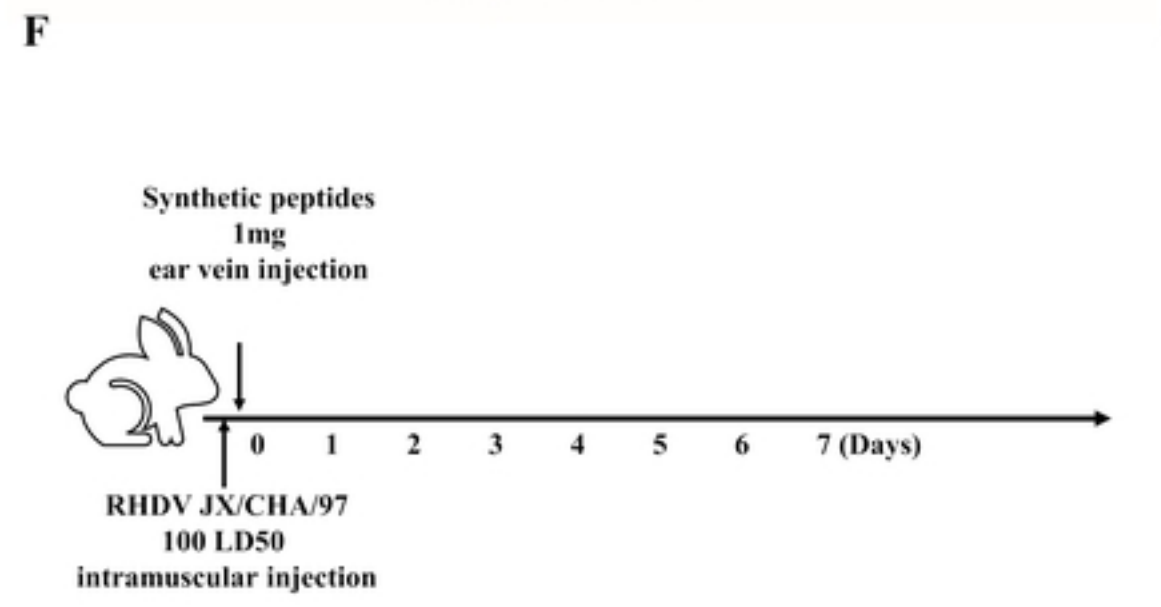

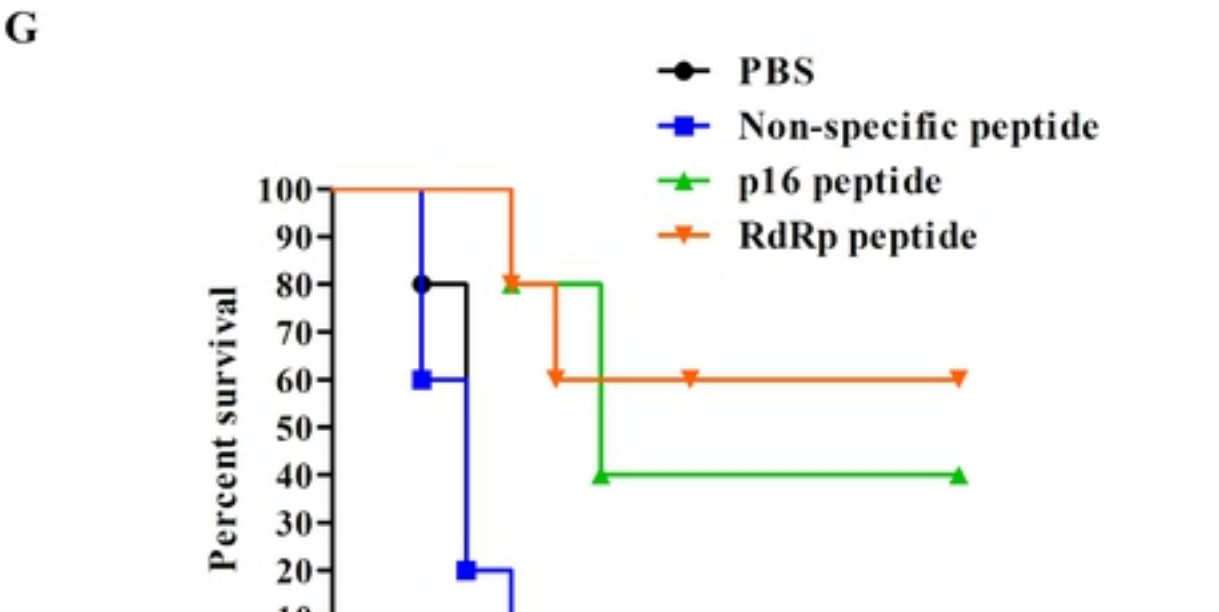

Fig 7

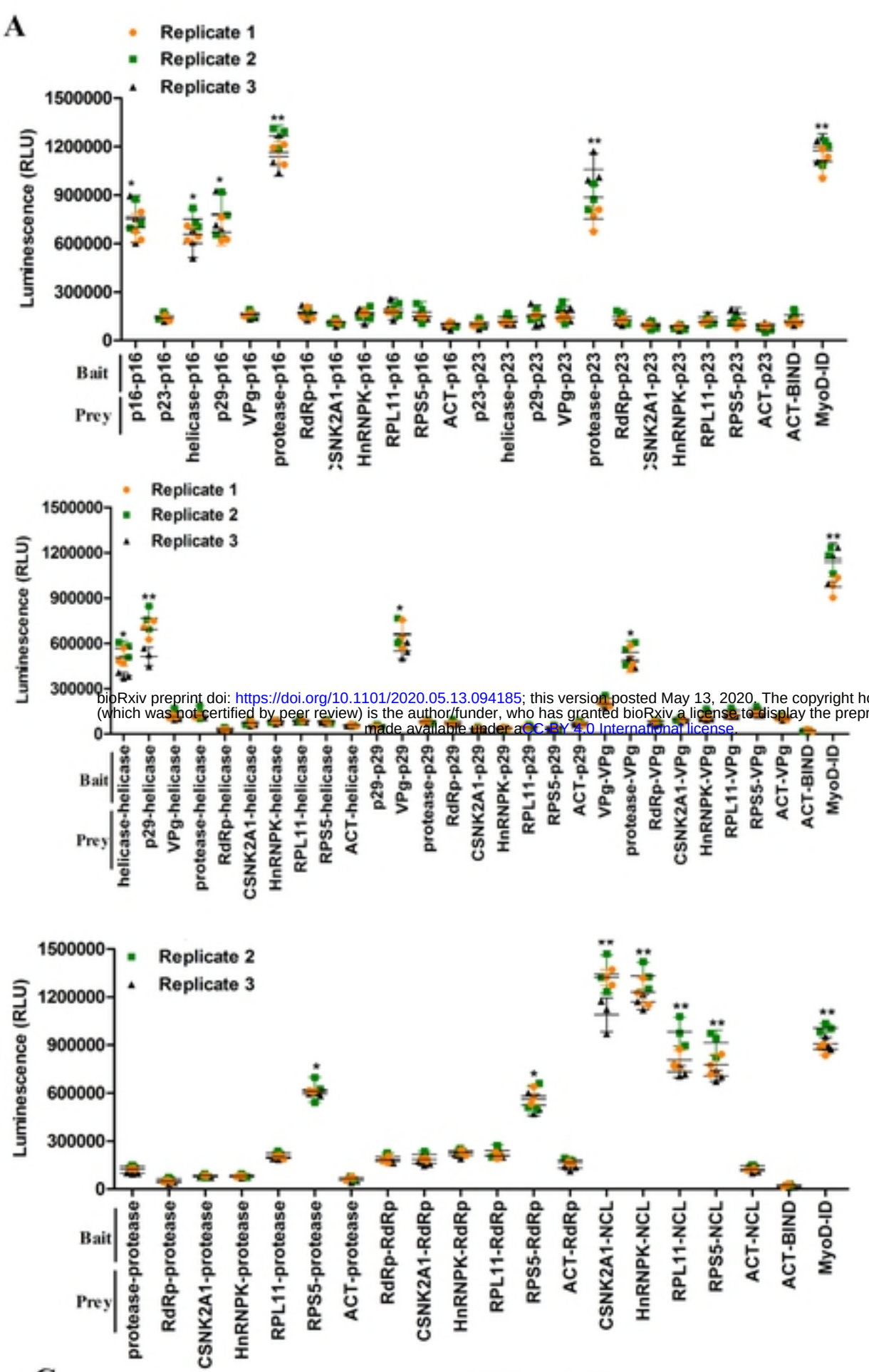

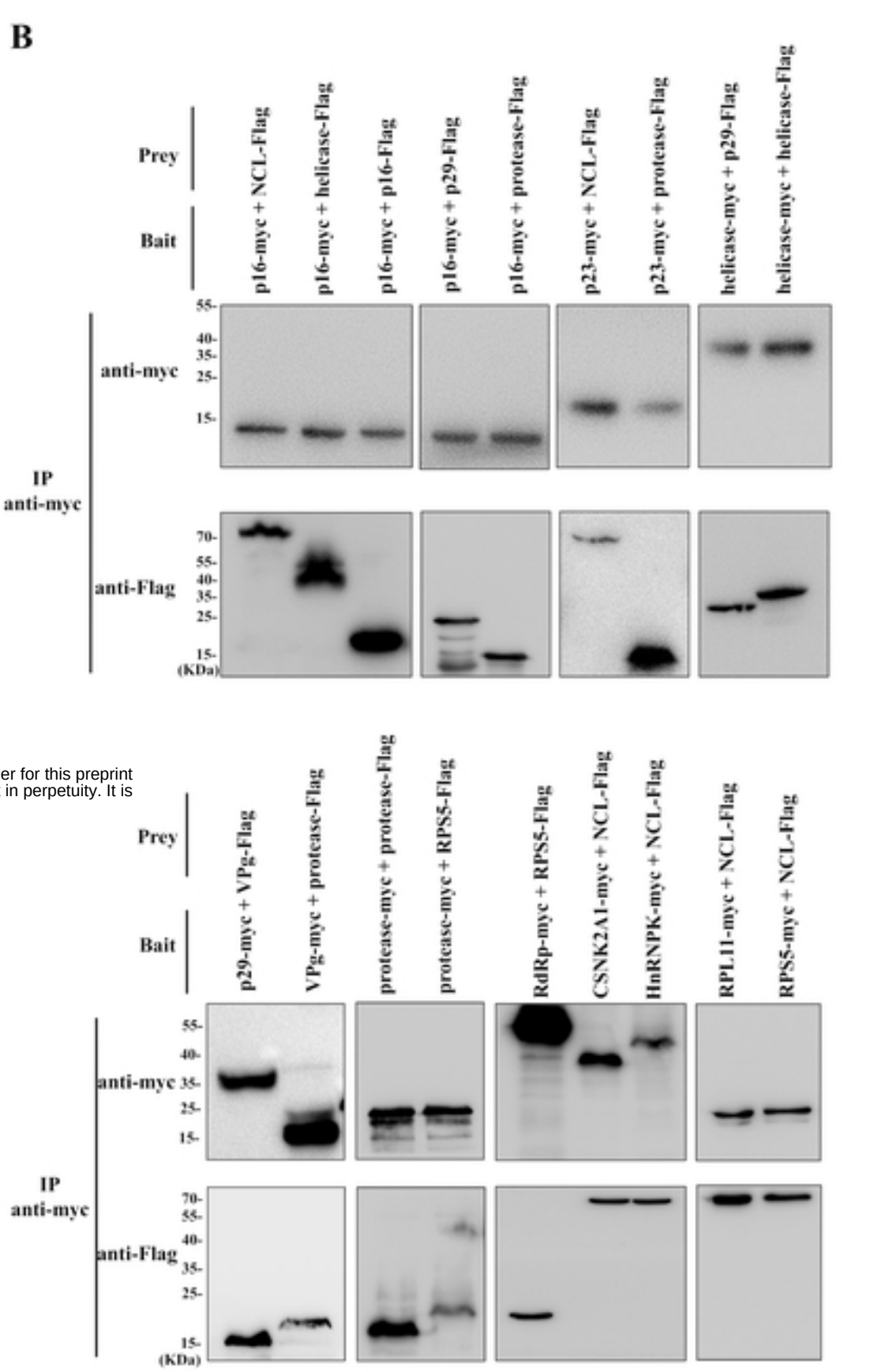

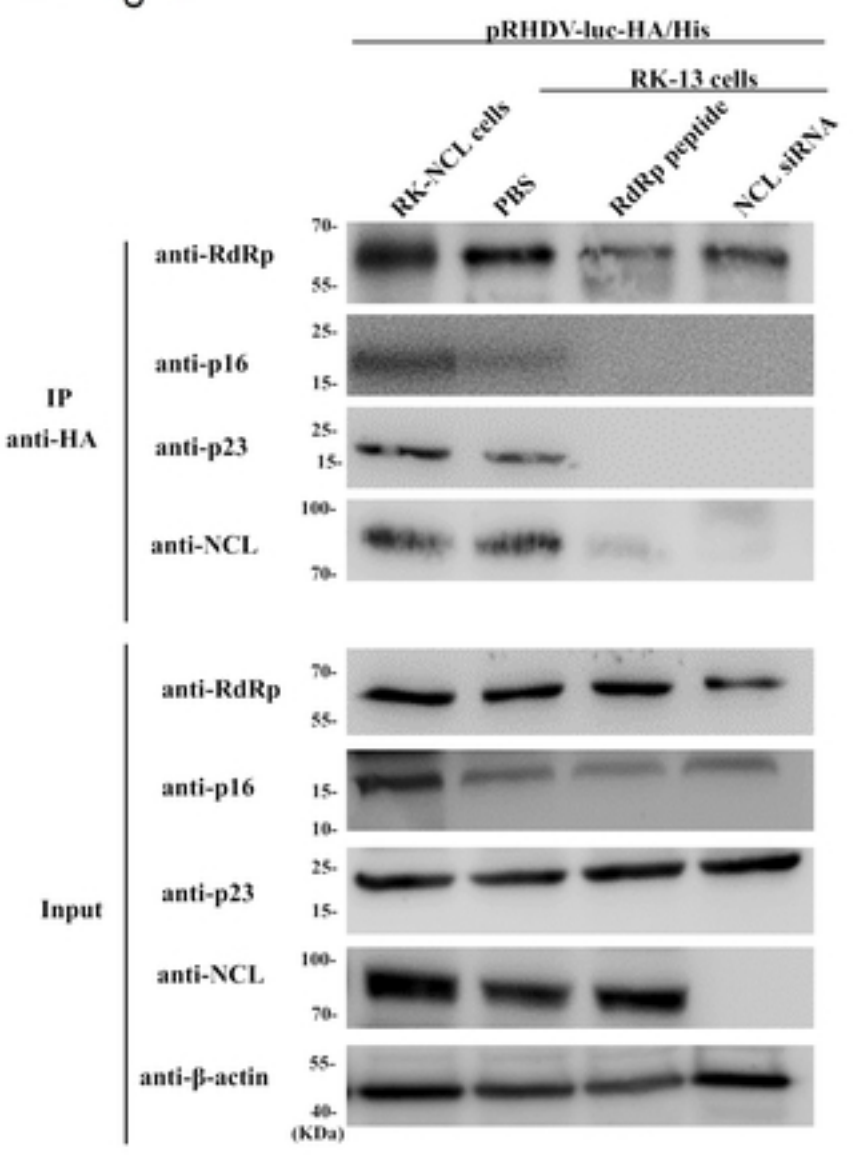

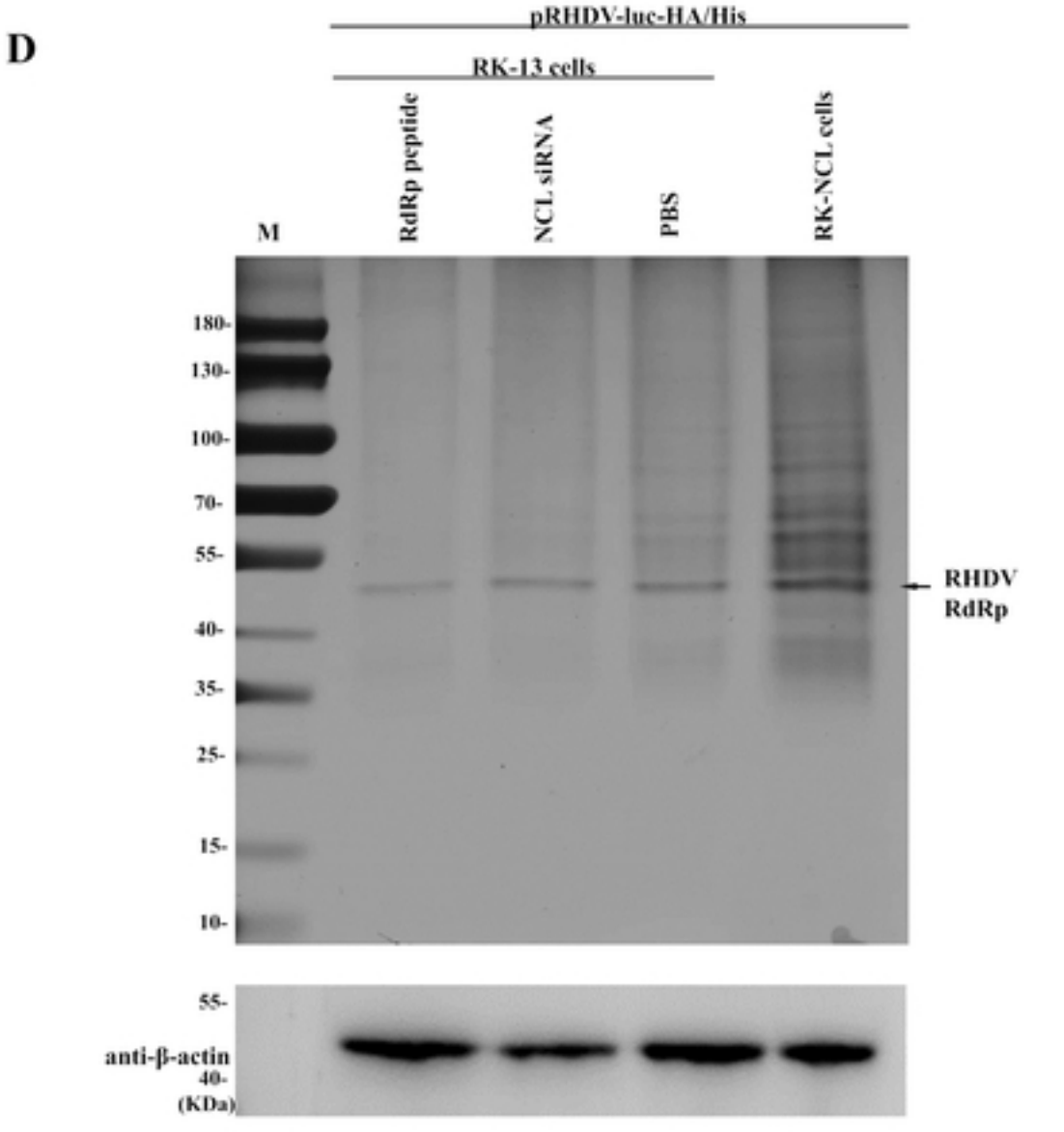

Fig 8

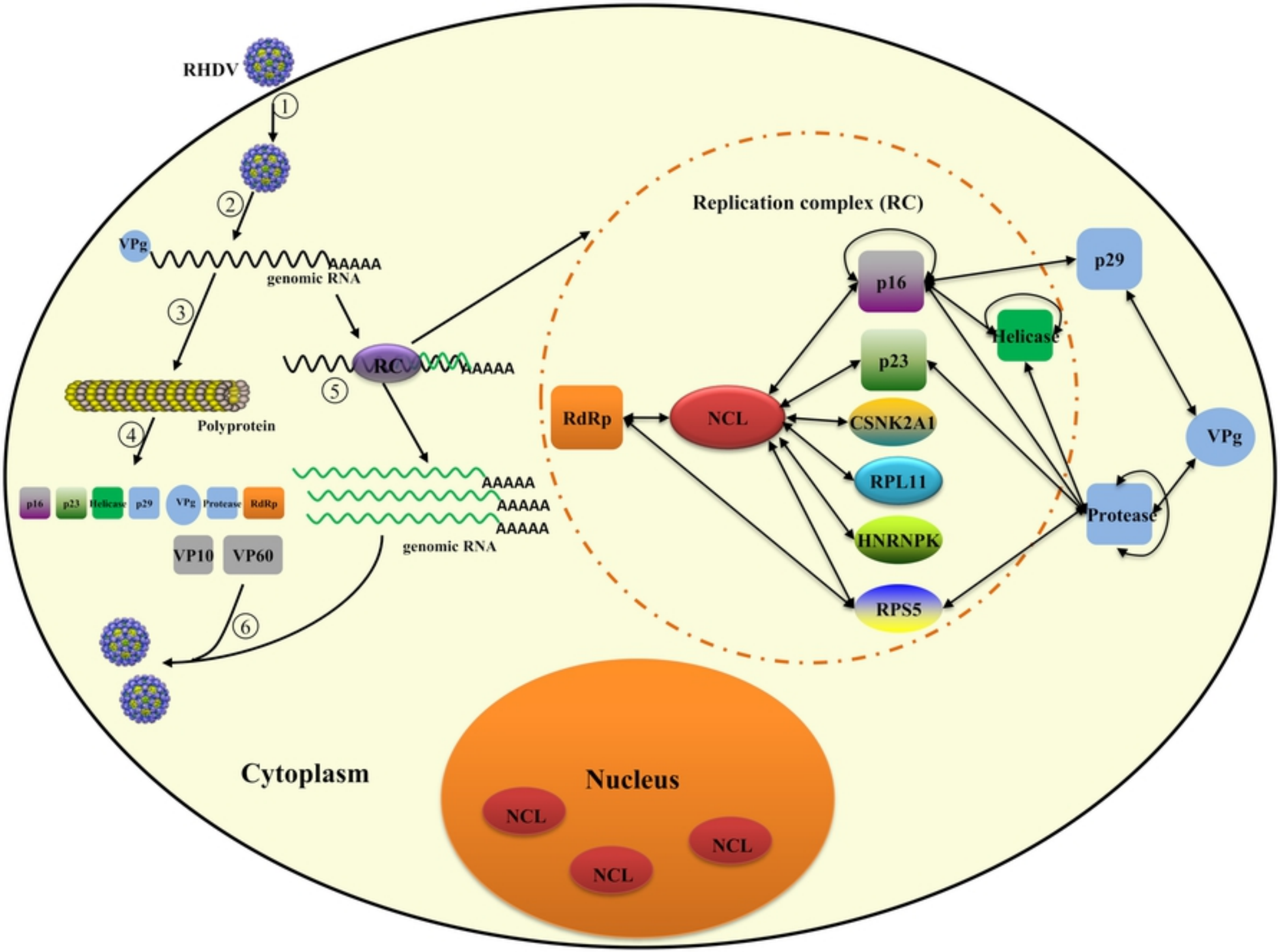
RHDV
1
2
VPg
AAAAA
genomic RNA
3
4
Polyprotein
p16
p23
Helicase
p29
VPg
Protease
RdRp
VP10
VP60
5
RC
AAAAA
AAAAA
AAAAA
AAAAA
genomic RNA
6
Cytoplasm
Nucleus
NCL
NCL
NCL
Replication complex (RC)
RdRp
NCL
p16
p23
CSNK2A1
RPL11
HNRNPK
RPS5
Helicase
p29
VPg
Protease

Fig 9